Layered Oxides as Potential Thermoelectrics

A Thesis

submitted to

Indian Institute of Science Education and Research Pune

in partial fulfilment of the requirements for the

BS-MS Dual Degree Programme

by

S.Vignesh

Indian Institute of Science Education and Research Pune

Dr. Homi Bhabha Road,

Pashan, Pune 411008, INDIA.

April, 2018

Supervisor: Dr. Sunil Nair

© Vignesh 2018

Certificate

This is to certify that this dissertation **Layered Oxides as Potential Thermoelectrics** towards the partial fulfilment of the BS-MS dual degree programme at the Indian Institute of Science Education and Research, Pune represents study/work carried out by **S.Vignesh** at Indian Institute of Science Education and Research under the supervision of **Dr. Sunil Nair**, Assistant Professor, Department of Physics, during the academic year 2017-2018.

Student
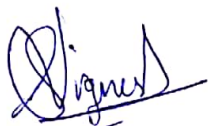S.Vignesh

Supervisor
Dr. Sunil Nair

Committee:

Dr. Sunil Nair

Dr. Prasenjit Ghosh

Declaration

I hereby declare that the matter embodied in the report entitled **Layered Oxides as Potential Thermoelectrics** are the results of the work carried out by me at the Department of Physics, Indian Institute of Science Education and Research, Pune, under the supervision of **Dr. Sunil Nair** and the same has not been submitted elsewhere for any other degree.

Student
S.Vignesh

Supervisor
Dr. Sunil Nair

Acknowledgements

Abstract

Thermoelectrics are devices that can convert waste heat into usable electrical energy. There is a longstanding challenge to synthesize materials with large conversion efficiencies and lower Cost per Watt ratios so that thermoelectricity can be a commercially viable source of energy. The chief candidates for thermoelectric application are intermetallic semiconductors but due to reasons like toxicity, stability and cost viability they have found very little success. But in recent years transition metal oxides have emerged as a possible alternative. Oxides as possible thermoelectric materials came into consideration after the discovery of large thermopower and low resistivity in the layered oxide $NaCo_2O_4$. Following this discovery layered oxide compounds like the Ruddlesden-Popper series have been of great interest in this area of research. In this project the La-Ni-O family of the Ruddlesden-Popper series are studied for their structural and thermoelectric properties. The general formula of this series is given as $La_{n+1}Ni_nO_{3n+1}$ and in this project the compounds La_2NiO_4 (n=1) and $La_3Ni_2O_7$ (n=2) along with a few compositions each with a Ca^{2+} dopant at the La^{3+} site was synthesized via solid state synthesis and studied for its thermoelectric properties. La_2NiO_4 has a tetragonal crystal structure with *I4/mmm* space group symmetry whereas $La_3Ni_2O_7$ has an orthorhombic crystal structure with *Fmmm* space group symmetry. Rietveld refinement was done using these space groups for the corresponding compounds to calculate the lattice parameters. High temperature X-Ray Diffraction analysis was also performed on some of the samples to look for any structural phase transition. Thermal conductivity measurements showed a decrease in thermal conductivity with increasing temperature for all samples and a general increase in thermal conductivity with increasing dopant concentration. Electrical resistivity is also observed to be decreasing with increasing temperature.

Contents

List of Figures

List of Tables

Chapter 1

Introduction

1.1 What are Thermoelectrics?

Thermoelectrics are a class of materials that can generate electricity from the application of a temperature gradient using the Seebeck effect. The Seebeck effect can be seen when there is a voltage produced in the presence of a difference in temperature between two different electrical conductors or semiconductors.
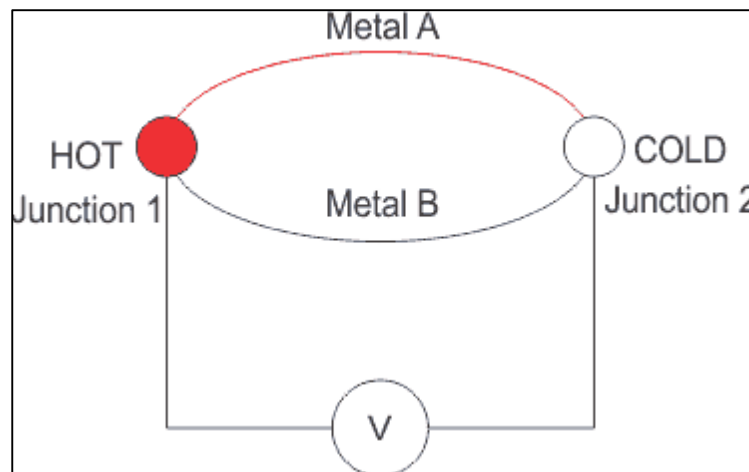
Fig. 1. Principle of Seebeck effect

When heat is applied to Junction 1, heated electrons from this junction start moving towards the cooler Junction 2. If this pair is connected together through an electrical circuit as seen in Fig. 1, a direct current is seen to flow through the circuit which generates a potential difference between the two junctions. The voltage produced by the Seebeck effect is minuscule, usually only a few microvolts per Kelvin of the temperature difference between the junctions. Some devices can produce a few millivolts when the temperature difference is large enough. Numerous such devices can be connected in series or parallelly in order to increase the output voltage or current respectively. The quantitative measure of the output voltage produced is given be the Seebeck Coefficient (also known as thermopower) $S = \frac{\Delta V}{\Delta T}$, where ΔV is the Seebeck voltage generated and ΔT is the difference in temperature between the 2 junctions.

The overall efficiency of a thermoelectric device is captured by a dimensionless figure of merit zT, given by

$$zT = \frac{S^2 \sigma T}{K}, where\ K = K_e + K_l.$$ (1.1)

Here S is the Seebeck Coefficient, σ is the electrical conductivity of the compound, T is the temperature and K is the thermal conductivity of the compound comprising of electronic and phononic parts (K_e & K_l respectively). The term $S^2\sigma$ is defined as the Power Factor of the material. Thermoelectric materials with $zT \approx 1$ are considered high performance materials with potential commercial applications. From the formula for the figure of merit, it can be seen that a good thermoelectric material needs to have a low thermal conductivity and large electrical conductivity and Seebeck Coefficient[1]. The maximum power generation efficiency (η) of a thermoelectric material is given by,

$$\eta = \left(\frac{T_{hot} - T_{cold}}{T_{hot}}\right)\left[\frac{\sqrt{1 + ZT_m} - 1}{\sqrt{1 + ZT_m} + \left(\frac{T_{cold}}{T_{hot}}\right)}\right]$$ (1.2)

where T_m is the mean temperature. The electrical conductivity (σ) is given in terms of the carrier concentration n as well as the carrier mobility μ by:

$$\sigma = ne\mu$$ (1.3)

where e is the charge of an electron. Fig. 2 shows the middle ground between large Seebeck coefficient and high electrical conductivity that needs to be achieved in order to enhance the overall figure of merit zT. As shown in Fig. 2, this peak generally occurs between carrier concentrations of 10^{19} and 10^{21} carriers per cm^3 which falls in the region of heavily doped semiconductors.

Glass, despite showing some of the lowest lattice thermal conductivities, cannot be a good thermoelectric as they lack the required electronic properties when compared with crystalline semiconductors. Thermoelectrics hence need a rather uncommon kind of material known as 'phonon-glass electron-crystal'[2]. The electron crystal condition arises since crystalline semi-conductors are the best in meeting the compromise in the electrical properties. The phonon-glass condition arises due to the requirement for as low a thermal conductivity as possible given that glass shows some of the lowest lattice thermal conductivities. In general, the ZT of a material is maximized either by increasing the Power Factor as much as possible or by reducing

its lattice thermal conductivity. Power Factor can be increased by choosing an appropriate dopant for a sample which could result in the increase in the charge carrier concentration or increase in Seebeck coefficient or both. This dopant has to be chosen such that the crystalline structure of the material is preserved while increasing the possibility of phonon scattering to disrupt the phonon path which reduces the lattice thermal conductivity.
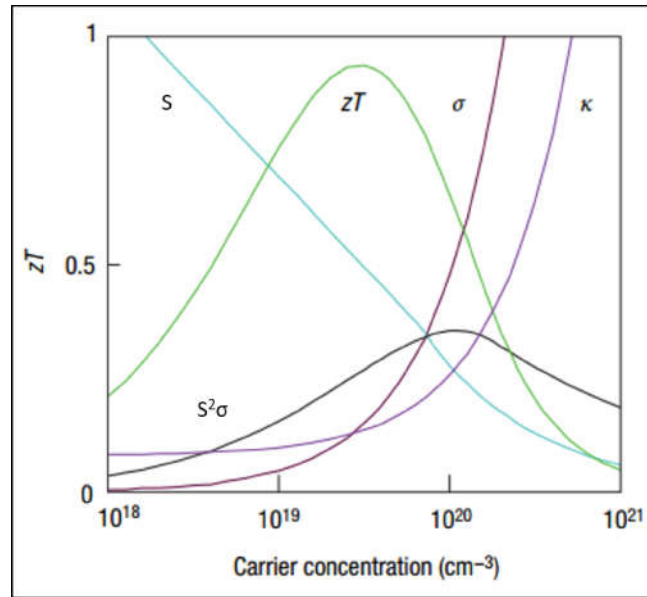
Fig. 2. Maximizing ZT by tuning the carrier concentration. Modelled from Bi_2Te_3 system.[1]

Metals are limited for this application due to the Wiedemann-Franz law which gives a fixed ratio between the electrical and thermal conductivity.

$$\frac{K}{\sigma} = LT, K = K_e \qquad (1.4)$$

where the Lorentz number $(L) = 2.44 \times 10^{-8}$ $J^2K^{-2}C^{-2}$.

Due to this, metals need to have large Seebeck Coefficients for them to work as viable thermoelectric materials. Semi-conductors on the other hand show a larger electrical to thermal conductivity ratio and also possess larger Seebeck Coefficients than metals. This coupled with their doping capabilities make semiconductors suitable candidates for thermoelectric materials.

One way to move around the conflict of phonon-glass and electron-crystal properties is to picture a complex material with separate regions catering to certain functions. This is called the substructure approach where a complex material is synthesized by stacking layers of substructures which can successfully preserve the crystalline structure while still reduce the

lattice thermal conductivity. A good example of a thermoelectric material that uses this approach is the Sodium Cobaltate oxide (Na_xCoO_2). [3][4]

The Seebeck coefficient of a material can be written as

$$S = \frac{8\pi^2 k_B^2}{3eh^2} m^* T \left(\frac{\pi}{3n}\right)^{2/3} \tag{1.5}$$

where e is the electron charge, k_B is the Boltzmann constant, h is the Planck's constant, m^* is the effective mass of the charge carrier and n is the carrier concentration. m^* is the density of states (DOS) effective mass. m^* increases in the presence of flat and narrow bands with a large density of states present at the Fermi surface. But, since the inertial mass of the charge carrier is also related to the effective mass, heavy charge carriers will have lower velocities that results in low mobility which in turn will reduce the electrical conductivity as seen in equation 1.3. This problem can be solved by using the nano-structuring approach which enhances the DOS near the Fermi level via quantum confinement that enhances the Seebeck coefficient. This approach also offers a way to decouple the electrical conductivity and Seebeck coefficient which works on the principle that the mean free path of the electrons is much smaller than that of the phonons. The nano-structuring presents a large number of interfaces in which phonons can be scattered more effectively and favourably than electrons over a large range of the mean free path. This reduces lattice thermal conductivity while the mobility and electrical conductivity are not altered.[5][6] The lattice thermal conductivity of the material can also be reduced, thereby enhancing zT, by the formation of superlattices. This occurs due to the increased phonon scattering due to the formation of numerous interfaces. This phenomenon has been observed clearly in the Sr-Ti-O Ruddlesden-Popper series which is a natural superlattice.[7]

1.2   Oxide Thermoelectrics

Oxides are generally poor candidates as thermoelectrics as they show large lattice thermal conductivity and low carrier mobility, due to the strong bonding of atoms with lower mass and large electronegativity of oxygen respectively. In spite of this they have been considered because of their relatively large Seebeck values at high temperatures which is due to the presence of a wider band gap. Hence the high zT values found in doped-ZnO[9]-[13], Na_xCoO_2[4] and the Ruddlesden-Popper series $A_{n+1}B_nO_{3n+1}$[8] are ground-breaking and has started the search for more oxide thermoelectrics. [3][14]

The structural flexibility, low cost and toxicity were also important factors for oxides to be considered as potential thermoelectrics. The structural flexibility also facilitates the use of the substructure approach which has proven to be effective in increasing the *zT* as shown by the Sodium Cobaltate oxides. The stability of oxides at high temperatures also ensures a high Carnot efficiency as given by equation 1.2. Layered oxides are better candidates due to their inherently low lattice thermal conductivity. These layered oxides can later be doped with the appropriate element to increase their electrical conductivity and thermopower. Fig. 3 shows the *ZT* values of some of the known Oxide thermoelectric materials.
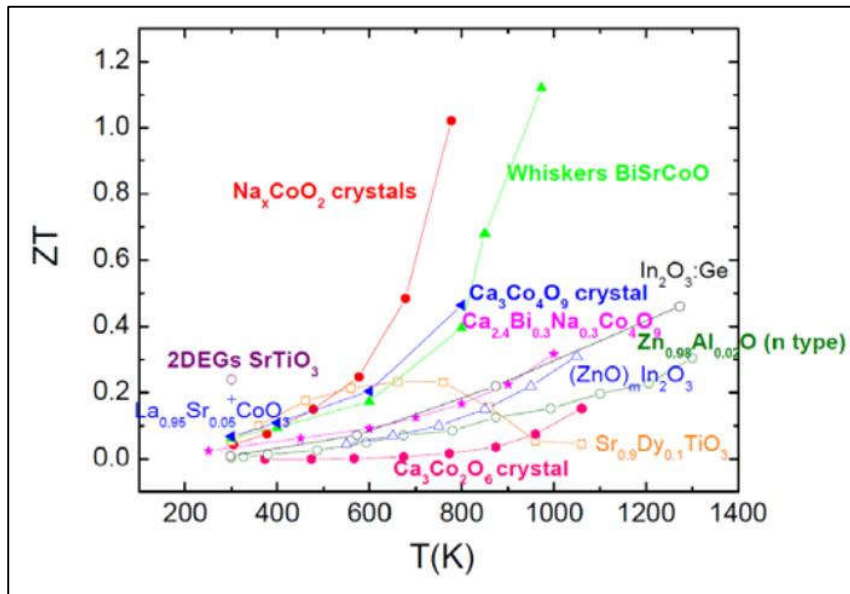
Fig. 3. *ZT* values of some of the known oxide thermoelectric materials. [15]

1.3 Ruddlesden-Popper Series

Ruddlesden-Popper phases are a kind of layered perovskites that have a structure similar to that of K_2NiF_4 and form a homologous series.[16][17][18] The general formula of RP phase is given by $A_{n+1}B_nO_{3n+1}$, where *A* and *B* are cations. This formula is also written as $AO(ABO_3)_n$ where ABO_3 is the perovskite and *n* is the number of layers of perovskite stacked between AO layers along the *c*-axis in the crystallographic plane. In the general formula of RP phases, $A_{n+1}B_nO_{3n+1}$, *A* generally represents an alkali, alkaline earth, or rare earth metal whereas *B* generally refers to a transition metal.

Ruddlesden-Popper phases are predominantly insulators and since they are a natural superlattice show very low thermal conductivity which is ideal for a thermoelectric material. The resistivity of the Ruddlesden-Popper series generally decreases as we go further up in the

series because of the increasing three-dimensional character. [19] This has been verified in the La-Ni-O ($La_{n+1}Ni_nO_{3n+1}$) family where the room temperature resistivity is seen to be decreasing as we go from n=2 to n=∞ in the series.[20] The electrical conductivity of the compound can be improved by doping it with the appropriate element.
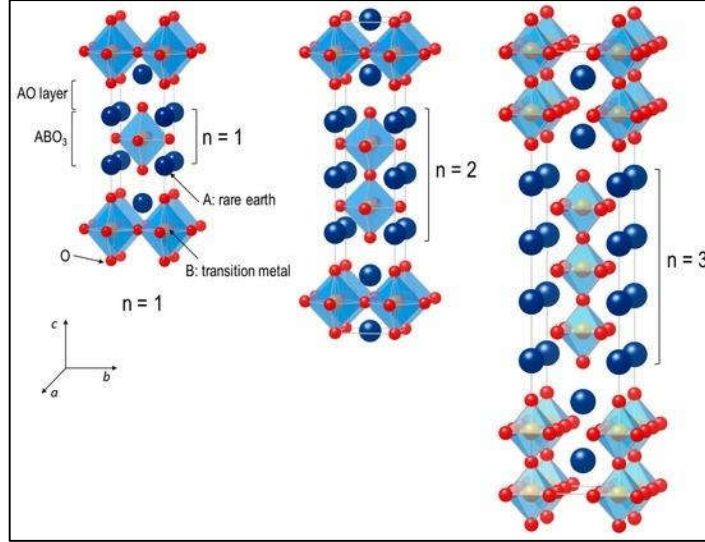
Fig. 4. Schematic of the Ruddlesden-Popper series

One such system from the Ruddlesden-Popper series that was studied for potential thermoelectric applications was the Strontium Titanites ($Sr_{n+1}Ti_nO_{3n+1}$)[7]. The dopant used in this system was Nb^{4+} in the Ti^{3+} site. The maximum *zT* achieved was 0.37 for the Nb-doped $SrTiO_3$ thin film ($SrTi_{1-x}Nb_xO_3$) at x=0.2[21]. Other systems such as Calcium Titanites (Ca-Ti-O) and Barium Titanites (Ba-Ti-O) were also studied for their potential thermoelectric properties.[22] The thermoelectric phase diagram of these compounds with Ti and Nb dopants are shown in Fig. 5.
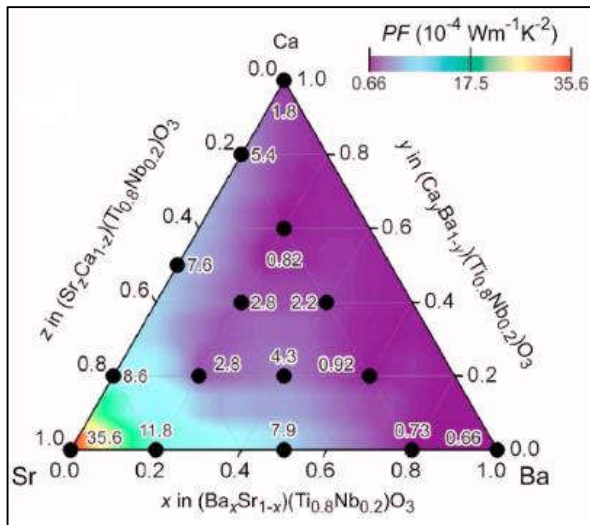
Fig.5. Thermoelectric Power Factor plotted for the (Ca, Sr, Ba) x ($Ti_{0.8}Nb_{0.2}$)O_3 films at room temperature[22]

This study shows that Calcium or Barium substitution in the $Sr(Ti_{0.7}Nb_{0.2})O_3$ negatively influence the thermoelectric properties of $Sr(Ti_{0.7}Nb_{0.2})O_3$.

1.4   Lanthanum Nickelates

The Lanthanum Nickelate (La-Ni-O) system was chosen due to its reported data on electrical conductivity and because of its well-studied structure. The general formula of this system is given by $La_{n+1}Ni_nO_{3n+1}$.
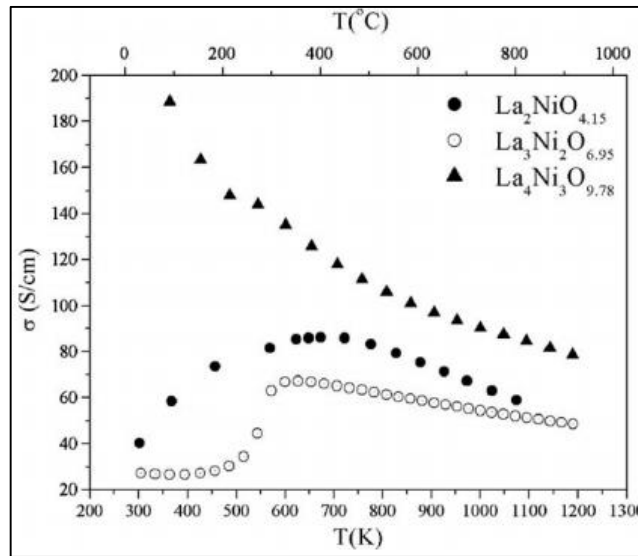
Fig. 6. Electrical conductivity plotted against the temperature for $La_2NiO_{4.15}$, $La_3Ni_2O_{6.95}$ and $La_4Ni_3O_{9.78}$ from 300K to 1173K in air. [23]

The thermal transport properties and the thermopower of this system at high temperatures were not reported so far and hence the thermoelectric properties of this system were unknown. Earlier reports of this series showed promising values of electrical conductivity in the parent compounds[20][23][24] which showed some increase in the presence of a dopant.[25]-[29]

1.5   Aim of the project

The objective of this project was to look for high efficient thermoelectric materials among layered oxides. To that effect, a few Lanthanum Nickelates were chosen to be synthesized since they have not yet been studied for their thermoelectric properties. The samples were synthesized using solid state synthesis and were verified by X-Ray Diffraction analysis at room temperature and EDX analysis. After successful sample synthesis, thermal properties and

electrical transport properties were measured in order to calculate the overall figure of merit zT of the samples. From the observed results, further investigation is being done on these Lanthanum Nickelates and other layered oxide compounds are also being studied for their thermoelectric properties.

Chapter 2

Experimental techniques

2.1 Synthesis

La_2NiO_4(n=1) and $La_3Ni_2O_7$(n=2) were the two parent compounds proposed to be synthesized. The dopant chosen after literature survey was Ca^{2+} at the La^{3+} site, the general formula of which can be written as $La_{2-x}Ca_xNiO_4$ [19] for n=1 and $La_{3-x}Ca_xNi_2O_7$ for the n=2 family. The compositions were decided to be 20 at.% (x=0.4 for n=1 and x=0.6 for n=2), 30 at.% (x=0.6 for n=1 and x=0.9 for n=2) and 40 at.% (x=0.8 for n=1 and x=1.2 for n=2) of Ca along with 10 at.% and 15 at.% for La_2NiO_4 (x=0.2 & 0.3 respectively) as well as 6.67 at.%, 10 at.% and 13.33 at.% for $La_3Ni_2O_7$ (x=0.2, 0.3 & 0.4 respectively). This results in a p-type doping where the holes act as the majority charge carriers. The stoichiometry of the dopant was chosen such that the compound retains its metallicity [16].

The compounds were prepared by solid state synthesis with stoichiometrically weighed La_2O_3(99.99%), NiO(99.99%) for the parent and $CaCO_3$(99.95%) for the doped samples. La_2O_3 was preheated for 5 hours at 900°C before weighing to remove any impurities. Stoichiometrically weighed La_2O_3, NiO, and $CaCO_3$ in the case of doped samples, were ground for 3 hours, pelletized and put in the furnace for heat treatment. The samples were initially heated at 1373K for 48hrs and the temperature was increased in subsequent steps up to 1473 after verifying with the La-Ni-O phase diagram [30]. Between each heat treatment samples were reground and pelletized. The 20 at.%, 30 at.% & 40 at.% doped

compounds of $La_3Ni_2O_7$ series were heated further to 1523K and 1573K for 48hrs each since the product wasn't formed at 1473K.

2.2 X-Ray Diffraction

Powder X-Ray diffraction patterns were taken at each step to follow the progress of the reaction. All XRD data was taken using Bruker D8 advance X-Ray Diffraction machine at IISER Pune. This facility uses *Cu-Kα* radiation with λ = 1.54056Å. Preliminary confirmation of formation of the product was done by comparing the acquired diffraction pattern with previously reported patterns. High temperature X-Ray Diffraction up to 1073K was also performed with certain samples (Undoped, 20 at.%, 30 at.% & 40 at.% of both families) to look for any kind of structural change at higher temperatures. The high temperature scans were done in vacuum and the samples were loaded on a Pt plate. Because of the use of a Pt plate instead of the standard sample holder some peaks of Pt were also observed in the scan. Rietveld refinement was done on the X-Ray Diffraction data using FullProf suite to extract the lattice parameters of each compound. In the refinement of the high temperature data three regions in the 2θ range were excluded as they contained the peaks of the Pt plate used.

2.2.1 Mathematical model of Rietveld refinement

Rietveld refinement is strongly dependent on the quantity which is being minimized in each iteration of the program which is given by equation 2.1 [31],

$$S_y = \sum_{y_i} w_i - (y_i - y_{ci})^2 \tag{2.1}$$

where sum is over all i^{th} step and the parameters are

S_y = Residual quantity which is refined,
y_i = Intensity observed in i^{th} step,
y_{ci} = Intensity calculated in i^{th} step,
w_i = $1/y_i$

Intensity calculated I_K for a Bragg peak K given by Miller indices (hkl) is dependent on the square of the absolute value of structure factor F_K. The structure factor is defined by equation 2.2 [31],

$$F_k = \sum_j N_j F_j \exp\left[2\pi i\left(hx_j + ky_j + lz_j\right)\right] \exp\left[-8\pi^2 u_{js}^2 \sin^2 \theta / \lambda\right] \qquad (2.2)$$

where u_{js} is defined as root mean square thermal displacement of jth atom in direction s parallel to the diffraction vector. [31]

h, k, l = Miller indices,
x_j, y_j, z_j = Position of jth atom in a unit cell,
N_j = Occupancy multiplier of jth atom,
F_j = Atomic form factor of jth atom

For a given powder diffraction pattern of a crystalline material, Bragg intensity at a specific step i will be dependent on all the intensity contributions from a specified angle in addition to the background intensity. y_{ci} is calculated based on equation 2.3 [31],

$$y_{ci} = s \sum_K L_K |F_K|^2 \phi(2\theta_i - 2\theta_K) P_K A + y_{bi} \qquad (2.3)$$

Parameters in the above equation are defined as

s = Scale factor,
K = Miller indices (hkl) for a given Bragg peak,
L_K = Lorentz polarization and multiplicity factors,
Φ = Bragg reflection profile function
P_K = Preferred orientation function,
A = Absorption factor,
F_K = Structure factor,
y_{bi} = Background intensity at i^{th} step.

Bragg reflection profile function φ gives each peak a shape which is calculated including instrumental corrections, asymmetry, sample displacement, transparency and size shape and strain effects. The full width half maximum (FWHM) (H) of a Bragg peak function is defined in equation 2.4 where U, V and W are parameters refined in the program.

$$H = \sqrt{U \tan^2\theta + V \tan\theta + W} \qquad (2.4)$$

2.2.2 Fitting criteria

The criteria to fit a given pattern depends upon the R values that are being used

in Rietveld refinement. R values helps to determine that if the fit has reached a global minimum and also it gives goodness of the fit. The complete set of R values can be seen in [18] Chapter 1 table 1.3. The most important of the R value is R-weighted pattern (R_{wp}) given by the equation 2.5 [31].

$$R_{wp} = \left[\frac{\sum w_i(y_i(obs) - y_i(cal))^2}{\sum w_i(y_i(obs))^2}\right]^{\frac{1}{2}} \tag{2.5}$$

To define the goodness of a fit we need to define the next important R value which is R-expected (R_e) given by equation 2.6 where N represents number of observations made and P represents number of parameters refined in a given cycle. Goodness of a given peak is the ratio of R-weighted pattern to R-expected equation 2.7 [31].

$$R_e = \left[\frac{N-P}{\sum w_i(y_i(obs))^2}\right]^{\frac{1}{2}} \tag{2.6}$$

$$S = \frac{R_{wp}}{R_e} \tag{2.7}$$

The goodness of a fit is quantitively given by how close it is to 1. In general, it is adequate to have a fit with goodness 1.3.

2.3 Thermal properties

The samples for measurement were prepared by being pressed into pellets with a diameter of ~13mm using a cold isostatic press and sintered at 1473K for 24 hours. High temperature thermal conductivity measurements up to 1073K were performed using LINSEIS LFA-1000 which gave the thermal diffusivity data for each sample.

The full schematic of the LFA-1000 apparatus is given in Fig. 7.
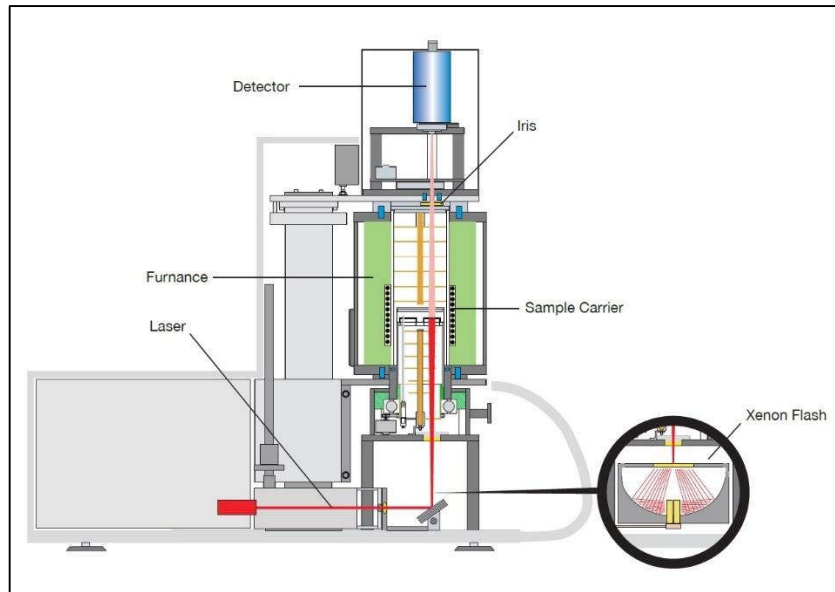
Fig. 7. Schematic of the Laser Flash Apparatus.[32]

The sample is positioned on a holder, which is surrounded by a furnace. For the measurement, the furnace is set to the inputted temperature and a programmable energy pulse irradiates the back side of the sample, resulting in a homogeneous temperature rise at the surface of the sample. The resultant rise in temperature at the surface of the sample is measured by a highly sensitive high-speed IR detector. Both, thermal diffusivity and specific heat can be determined from the temperature vs. time data. If the density (ρ) of the sample is known, the thermal conductivity can be calculated using the formula:

$$K = \alpha(T).\rho(T).C_p(T) \qquad (2.8)$$

where α is the thermal diffusivity of the sample at a particular temperature, ρ is the calculated density and C_p is the specific heat of the sample.

The density of the sample is computed by measuring the mass of the sintered pellet in a weighing scale (least count 0.1mg) up to 4 significant digits and calculating the volume of the sintered pellet by measuring its dimensions using a Vernier Calliper (least count 0.01mm). The error in computing the density has been estimated and has been propagated in the calculation of the thermal conductivity of the sample. Density of a material significantly affects its thermal conductivity as higher density implies that the molecules are more closely packed which facilitates transfer of heat through the molecules by collision thereby increasing the thermal conductivity of the material. Certain exceptions in this phenomenon are observed due to the presence of more phonon scattering mechanisms. The computed density of the sintered sample of La_2NiO_4 is ~74% of the theoretical value.[33] The theoretical density value of $La_3Ni_2O_7$ could

not be found during the survey. This implies that the measured values of thermal conductivity are lower than what is expected due to the lack of a denser sample.

The thermal diffusivity of the sample is measured by first determining the baseline and maximum rise to give the temperature difference, ΔT_{max}. Then the system calculates the time taken by the sample surface to reach said temperature. This is known as Half-time ($t_{1/2}$). The diffusivity is the calculated from the formula,

$$\alpha = 0.13879 \, L^2 / t_{1/2} \qquad (2.9)$$

where L is the thickness of the sample pellet. A schematic of this principle can be seen in Fig. 8.
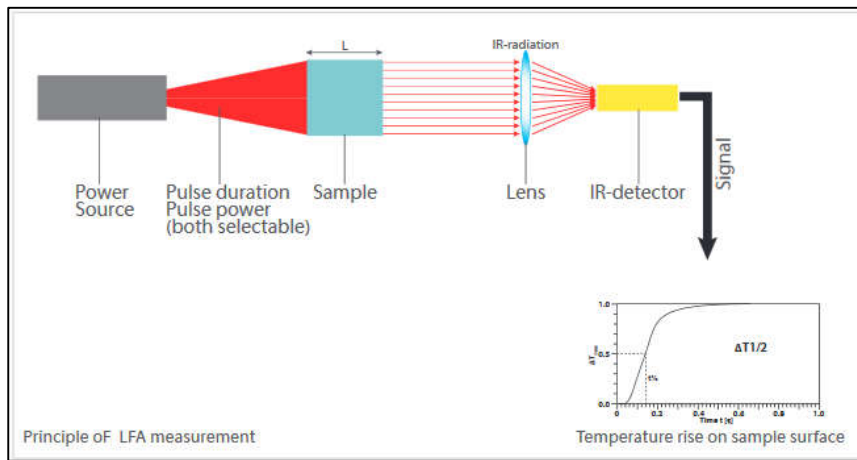
Fig. 8. Principle of LFA measurement.[32]

All measurements were done in vacuum and 3 data points were taken at every 50K intervals up to 1073K where the furnace heating rate was maintained at 10K/min. The specific heat used in equation 2.8 was taken from the work done by M. Castro et al. [34] for the La_2NiO_4 family and the study done in the dissertation by Nuri Solak [35] for the $La_3Ni_2O_7$ family. The room temperature specific heat values were used for the entire temperature range since there was no high temperature C_p measurement done for either of the compounds.

2.4 Electrical Properties

The Seebeck and electrical resistivity values at high temperatures up to 1073K of the samples were measured using LINSEIS LSR-3. A schematic of the apparatus is given in Fig. 9.
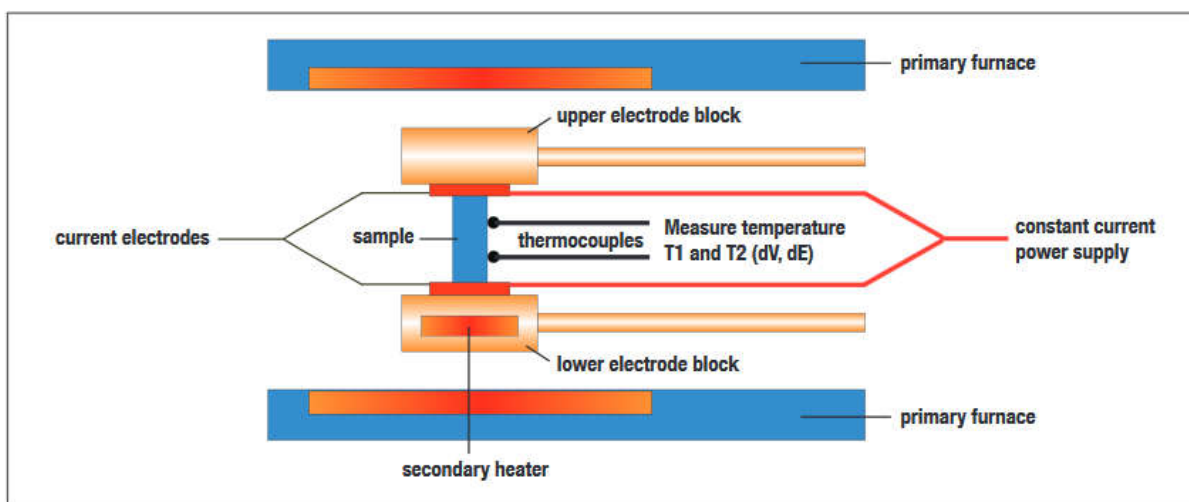
Fig. 9. Schematic of the LINSEIS LSR-3 Sample chamber.[36]

A sample of either cylindrical or cuboidal shape is placed vertically between two Platinum electrodes. The lower electrode block has an inbuilt heater and the entire setup is located in a furnace. The furnace around the setup heats the sample to a set temperature. At this temperature, the heater present in the lower electrode block generates a temperature gradient. The two thermocouples that are in contact with the sample measure this temperature gradient. The dc four-probe technique is employed to measure the electrical resistance of the sample by applying a constant current supply through both ends of the sample and determining the change in voltage between the wires present at each of the two thermocouples. The experimental uncertainty in the measurement has been taken as ±5% for the resistivity measurements and ±12% for the Seebeck measurements after referring to earlier reports[37]-[39]. This error has been propagated in the Power Factor and Electronic thermal conductivity calculations.

The Lanthanum Nickelate compounds were cut into cuboid shaped samples for this measurement with dimensions of approximately 2.5mm x 2mm x 11mm. Measurements were done in a Helium gas environment for the entire La_2NiO_4 (n=1) series while for the $La_3Ni_2O_7$ (n=2) series measurements were done only for the undoped and the 20 at.% Ca-doped samples due to unavailability of the instrument.

Chapter 3

Results and Discussion

In this chapter, all the acquired data on the synthesized compounds are reported and analysed.

3.1 La$_2$NiO$_4$ Family

3.1.1 Structural Analysis

The structure of the parent compound La$_2$NiO$_4$ was analysed using Rietveld refinement of the X-Ray Diffraction pattern of the sample. The pattern did not show any extra phases present and hence we can say that the synthesized compound is a phase pure compound. The La$_2$NiO$_4$ phase exists in the tetragonal I4/mmm space group and this has been used to perform the Rietveld refinement for the room temperature as well as the high temperature X-Ray Diffraction patterns. Fig. 10 shows the Rietveld refinement fit of the powder X-Ray Diffraction pattern of La$_2$NiO$_4$ taken at 296K and Fig. 11 shows the Rietveld refinement fit of the powder X-Ray Diffraction pattern of La$_2$NiO$_4$ taken at 373K.

Fig. 10. Rietveld refinement fit (black line) of the powder X-Ray Diffraction pattern (red circles) of La$_2$NiO$_4$ at 296K. Blue stripes indicate the peak positions of La$_2$NiO$_4$ and the blue line is the difference in the data and the fit.
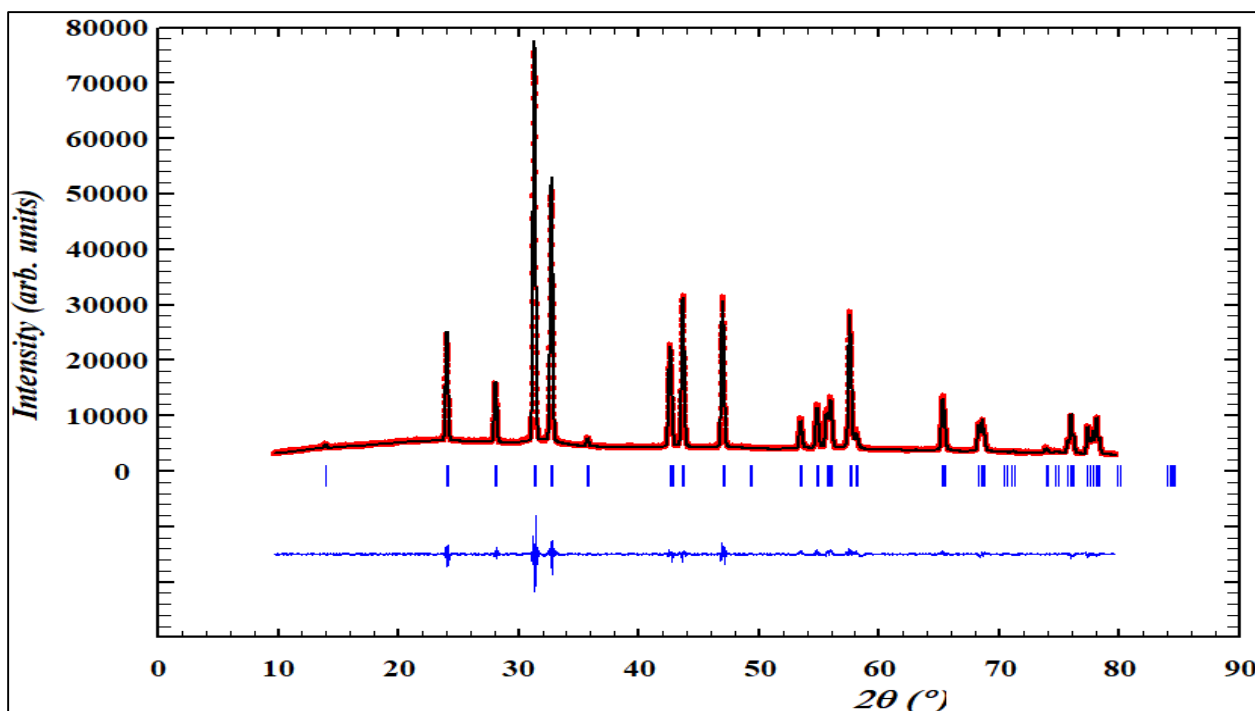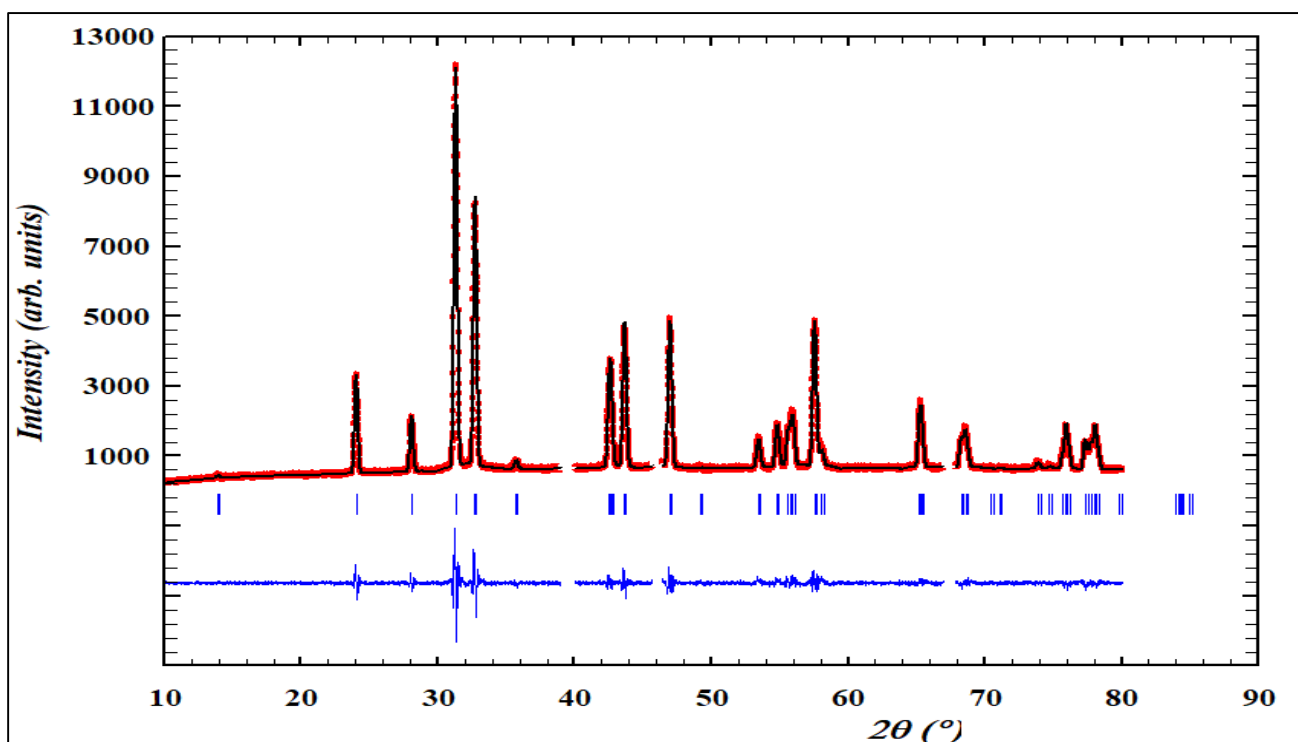
Fig. 11. Rietveld refinement fit (black line) of the powder X-Ray Diffraction pattern (red circles) of La₂NiO₄ at 373K. Blue stripes indicate the peak positions of La₂NiO₄ and the blue line is the difference in the data and the fit.

Table I shows the calculated parameters from the Rietveld refinement of the diffraction data of La₂NiO₄ at 296K. Certain regions are excluded as they contained peaks from the Pt plate used while performing the scan. Table III shows the calculated parameters from the Rietveld refinement of the diffraction data of La₂NiO₄ at 373K.

The atomic positions and fractional occupancy of La₂NiO₄ at 296K are given in Table II and the same for 373K is given in Table IV. The last digit in atomic positions and the last two digits in the fractional occupancy are uncertain. From the values of fractional occupancy calculated in both the scans we can say that the compound might have an excess of oxygen present in its stoichiometry the concentration of which increases with temperature.

After refining the structures of all the doped compounds in this family it was confirmed that all the compounds except the 40 at.% doped compound were devoid of any impurities. The 40 at.% doped compound contained 1.94% of NiO present in the sample.

Table I. X-Ray Diffraction data of La_2NiO_4 at 296K

Chemical Formula Molecular Weight (in g/mol) Temperature (K)	La_2NiO_4 400.51 296
Crystal Structure	Tetragonal
Space group symmetry	I4/mmm
Unit Cell Parameters	
a (Å)	3.865(2)
b (Å)	3.865(2)
c (Å)	12.696(6)
α, β, γ (º)	90
V (Å^3)	189.688
Diffraction angle, 2θ (º)	10-79.9957
Step size, 2θ (º)	0.01038
R values	
R_{wp}	7.26
R_e	3.29
χ^2	4.92
Goodness of fit	2.21

Table II. Atomic positions and fractional occupancy in La_2NiO_4 at 296K.

Atom	a	b	c	Fractional Occupancy
La1	0	0	0.3600(4)	1.570(62)
Ni1	0	0	0	0.716(04)
O1	0	0.5	0	2.017(66)
O2	0	0	0.1731(6)	3.524(20)
O3	0	0.5	0.2041(6)	1.255(47)

Table III. X-Ray Diffraction data of La_2NiO_4 at 373K

Chemical Formula Molecular Weight (in g/mol) Temperature (K)	La_2NiO_4 400.51 373
Crystal Structure	Tetragonal
Space group symmetry	I4/mmm
Unit Cell Parameters	
a (Å)	3.865(4)
b (Å)	3.865(4)
c (Å)	12.697(0)
α, β, γ (º)	90
V (Å^3)	189.709
Diffraction angle, 2θ (º)	10-79.9957
Step size, 2θ (º)	0.01038
R values	
R$_{wp}$	12.6
R$_e$	7.35
χ^2	2.93
Goodness of fit	1.71
Excluded regions, 2θ (º)	39-40 45.75-46.35 67-67.8

Table IV. Atomic positions and fractional occupancy in La_2NiO_4 at 373K.

Atom	a	b	c	Fractional Occupancy
La1	0	0	0.3606(4)	2.289(76)
Ni1	0	0	0	1.160(33)
O1	0	0.5	0	3.345(59)
O2	0	0	0.1717(8)	4.44(16)
O3	0	0.5	0.1967(8)	1.180(62(

Similar refinement was done for the same compound for the high temperature scans. The temperature was varied from 373-1073K with a 100K interval while the scan parameters remained the same. From this refinement we were able to calculate the lattice parameters at different temperatures. Fig.12 and Fig.13 shows the variation of lattice parameter *a* and *c* respectively with temperature.
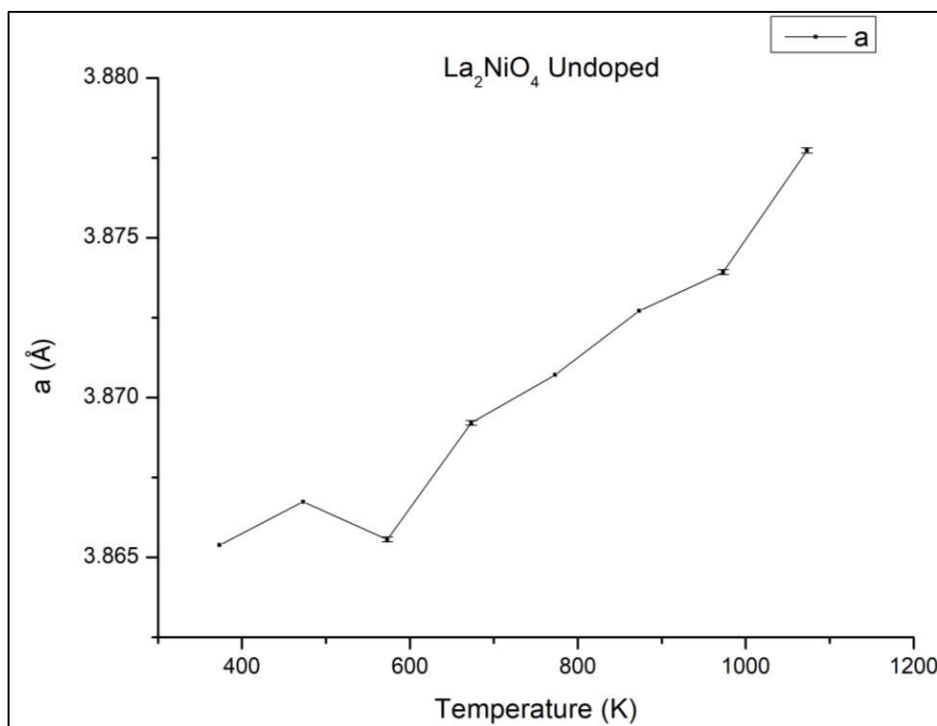

Fig. 12. Lattice parameter *a* vs. Temperature for La_2NiO_4.
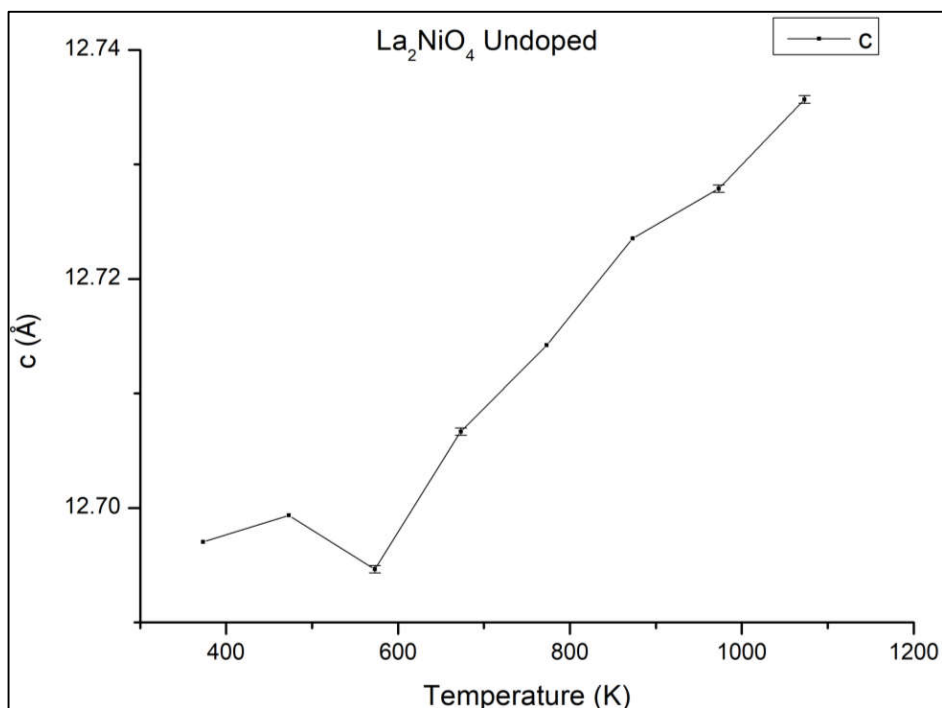

Fig. 13. Lattice parameter *c* vs. Temperature for La_2NiO_4.

From the above figures there seems to be a structural change occurring at 573K. This might be due to the evolution of oxygen from the lattice as the temperature increases. An overlay of the high temperature scans of the parent compound (Fig. 14.) shows that there is no structural phase transition in this compound.
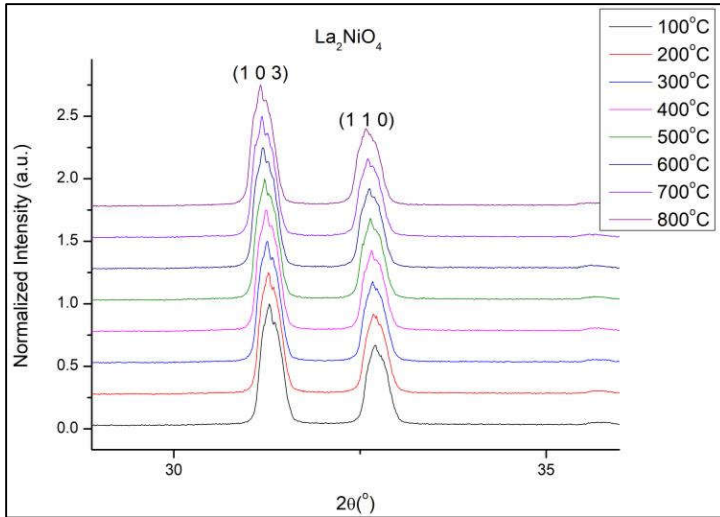

Fig. 14. High temperature XRD of La_2NiO_4 undoped compound with the corresponding (hkl) planes

3.1.2 Electrical properties

The electrical resistivity and the Seebeck coefficient of the La_2NiO_4 family of compounds was measured as mentioned in the experimental section earlier. The average resistivity values are shown in Fig. 15 and the average Seebeck Coefficient values are shown in Fig. 16.

3.1.2.1 Electrical Resistivity

Earlier reports of conductivity data for the parent compound[23] show a decrease in resistivity up to ~650K and an increase in the same beyond 650K up to ~1100K. The measured agrees with the reported measurements. The presence of Ca dopant has been reported to increase the electrical conductivity, i.e., decrease the resistivity.[23][24] However, that is not seen in this case. This might be the effect of the non-stoichiometry of oxygen in the system which could have changed the lattice parameters that might result in the decrease in the mobility of the charge carriers. This statement cannot be confirmed without verifying the oxygen content present in the compound. The decrease in the resistivity of the 40 at.% doped compound from the 30 at.% doped compound might be because change in mobility of the charge carriers due to excessive

doping of Ca on the parent compound. High temperature Hall measurement can be used to verify this.
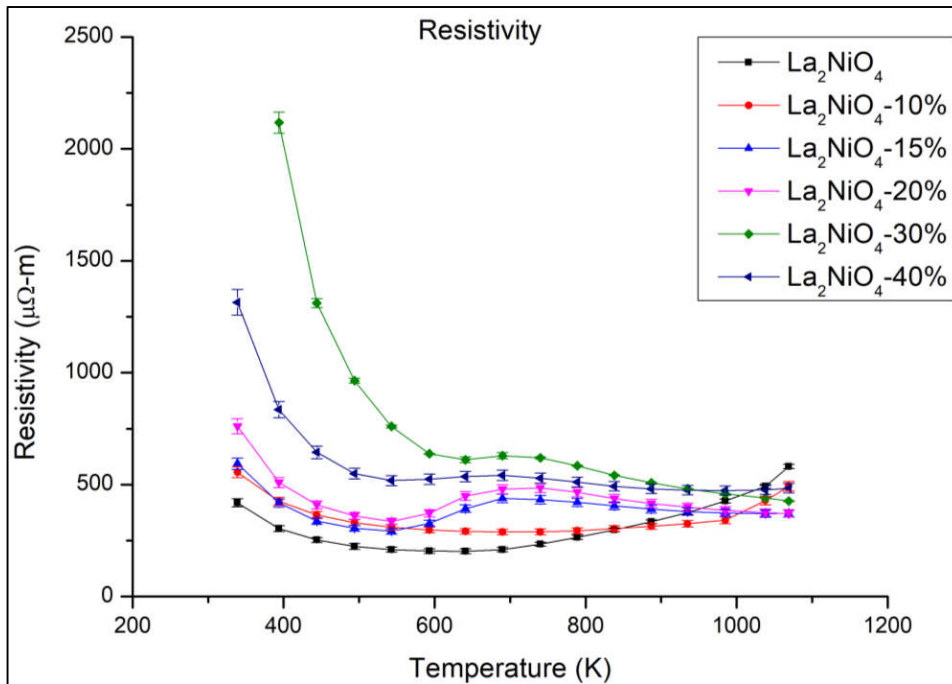

Fig. 15. Electrical resistivity at high temperatures for the La$_2$NiO$_4$ family of compounds.
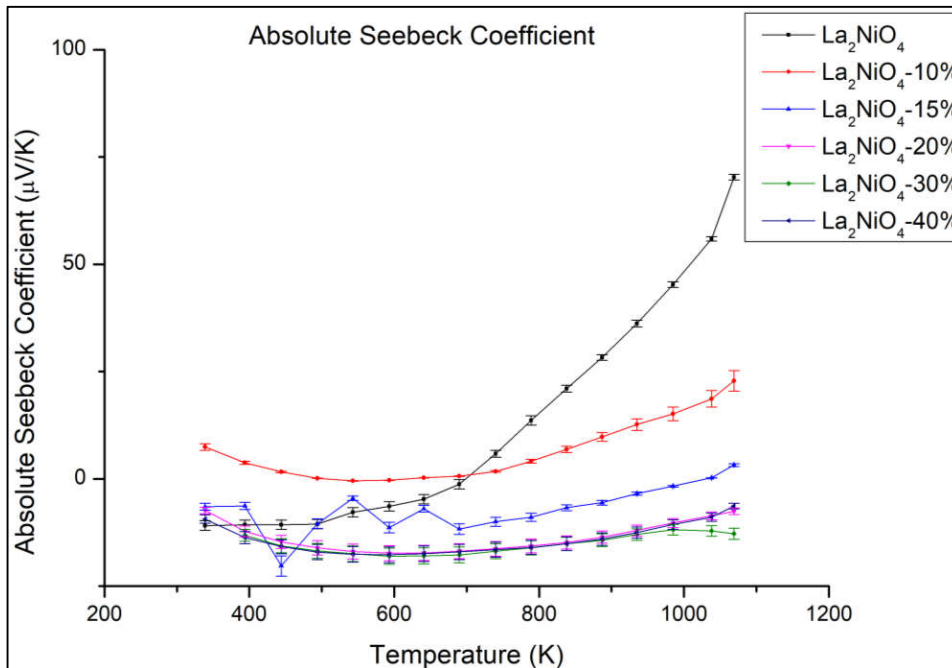
3.1.2.2 Seebeck Coefficient

Fig. 16. Absolute Seebeck Coefficient at high temperatures for the La$_2$NiO$_4$ family of compounds.

The presence of Ca dopant, despite being a p-type dopant, has considerably reduced the values of the Seebeck coefficient instead of increasing it as was intended. The fully negative values of Seebeck for the 40 at.% doped compound might be the result of NiO present in the sample. Increasing the dopant concentration might have introduced some defect in the system or reduced the charge carrier concentration or mobility or both since the Seebeck values are seen to decrease steadily with increasing dopant concentration. A high temperature Hall measurement is necessary to study the effects of dopant concentration and change in temperature in the carrier concentration and the mobility of the charge carriers. The maximum value of Seebeck coefficient is observed by the parent La_2NiO_4 compound at ~1073K with a value of 70.28 µV/K.

3.1.2.3 Power Factor

The Power factor is calculated using the formula

$$P.F. = \frac{S^2}{\rho} \qquad (3.1)$$

where S is the Absolute Seebeck coefficient and ρ is the electrical resistivity measured earlier. Fig. 17 shows the value of the Power Factor calculated from the Resistivity and Seebeck measurement done earlier.
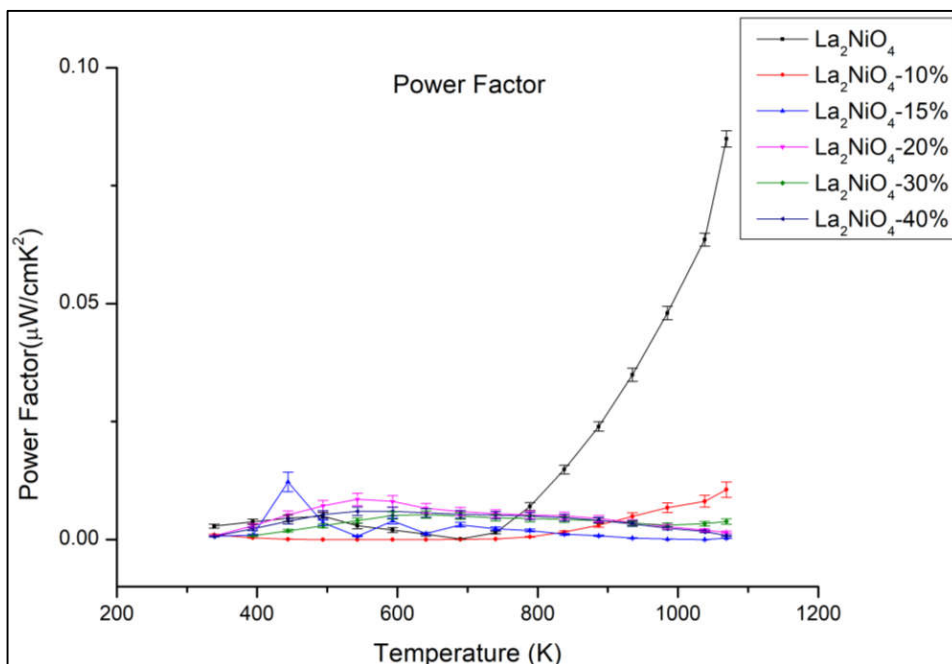

Fig. 17. Power Factor calculated at high temperatures for the La_2NiO_4 family of compounds.

The Power Factor of the doped compounds is almost constant throughout the temperature range and has very little variation across the dopant concentration. This implies that the carrier concentration of the doped compounds has not changed significantly by changing the dopant concentration contrary to what was intended. High temperature Hall measurement of these samples will shed more light to explain this behaviour. The maximum value of the Power Factor is seen in the parent compound with a value of 0.085 μW/cmK^2 at 1069K.

3.1.3 Thermal Properties

The average values of total thermal conductivity values are shown in Fig. 18. The heat capacity value used in this calculation was 170 JK^{-1}mol^{-1} taken from the study done by M. Castro et al. [34]

3.1.3.1 Total Thermal Conductivity

The total thermal conductivity (K_{total}) is the sum of the electronic thermal conductivity (K_e) and the lattice thermal conductivity (K_l). The values were calculated using equation 2.8 from the measured thermal diffusivity values and density of the sample.
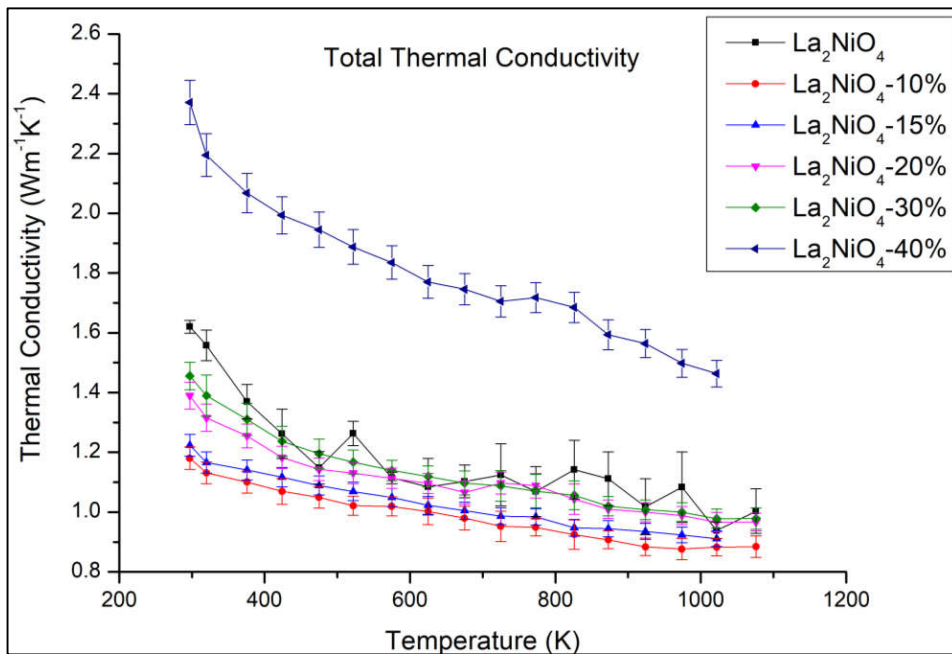

Fig. 18. Total thermal conductivity measured and calculated at high temperatures for the La$_2$NiO$_4$ family of compounds.

K_{total} is seen to be decreasing steadily with increasing temperature. Doping concentrations up to 30 at.% reduces the thermal conductivity values when compared with the corresponding

values of the parent compound but 40 at.% Ca doped compound shows a drastic increase in the thermal conductivity which might be due to the presence of trace NiO in the compound. Apart from that, Ca doping has successfully reduced the thermal conductivity of the series. This could be due to point defects in the system caused by the introduction of Ca dopant which scatter the phonons. The systematic change in lattice parameters with increasing dopant concentration might have produced new pathways for phonons to flow which could be the reason for the systematic increase in the thermal conductivity as we increase the dopant concentration.

3.1.3.2 Electronic Thermal Conductivity

K_e was calculated using the formula

$$K_e = \frac{LT}{\rho} \, Wm^{-1}K^{-1} \qquad (3.2)$$

derived from equation 1.3 where T is the temperature, ρ is the electrical resistivity and L is the Lorentz number which has a value of 2.44 x 10^{-8} $J^2K^{-2}C^{-2}$. Fig. 19 shows the plot of K_e against temperature calculated for the La_2NiO_4 family.

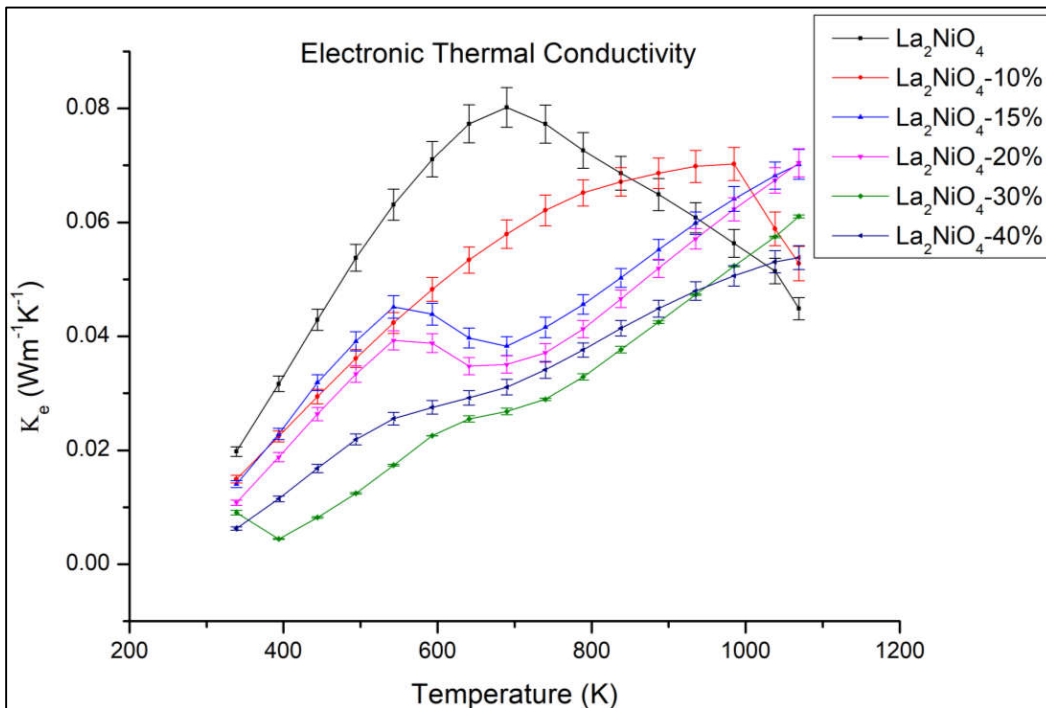**Fig. 19.** Electronic thermal conductivity (K_e) calculated at high temperatures for the La_2NiO_4 family of compounds.

The low value for the parent compound when compared with the total thermal conductivity could be due to the inherent lack of electrons in the system. The presence of the Ca dopant has reduced the electronic thermal conductivity as Ca was added as a p-type dopant with holes as

the majority charge carriers which reduced the concentration of electrons. Increase in the dopant concentration decreases the electronic thermal conductivity except for the 40 at.% Ca-doped compound. This behaviour of the 40 at.% doped compound can be the result of the presence of NiO. High temperature hall measurement can explain the change in the electronic thermal conductivity observed in all the compound at higher temperatures.

3.1.3.3 Lattice Thermal Conductivity

Lattice thermal conductivity (K_l) is the difference between K_{total} and K_e. Fig. 20 shows the calculated values of K_l. K_l decreases steadily with increasing temperature for all the compounds. Reduction in lattice thermal conductivity in the presence of Ca dopant could be the result of point defects present in the system. The systematic change in lattice parameters with increasing dopant concentration might have produced new pathways for phonons to flow which could be the reason for the systematic increase in the thermal conductivity as we increase the dopant concentration. From this plot it is clear that lattice thermal conductivity is more prominent in this system than electronic thermal conductivity.
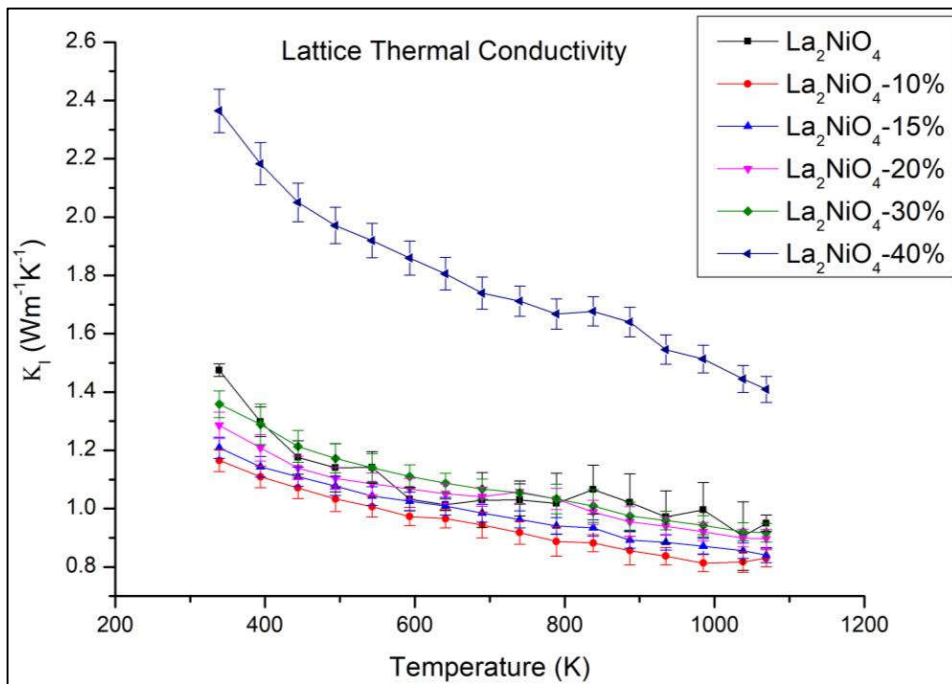

Fig. 20. Lattice thermal conductivity (K_l) calculated at high temperatures for the La_2NiO_4 family of compounds.

3.1.4 Figure of Merit zT

The overall figure of merit zT of the compounds is calculated using the formula given in equation 1.1. The calculated values of zT for this family are shown in Fig. 21.
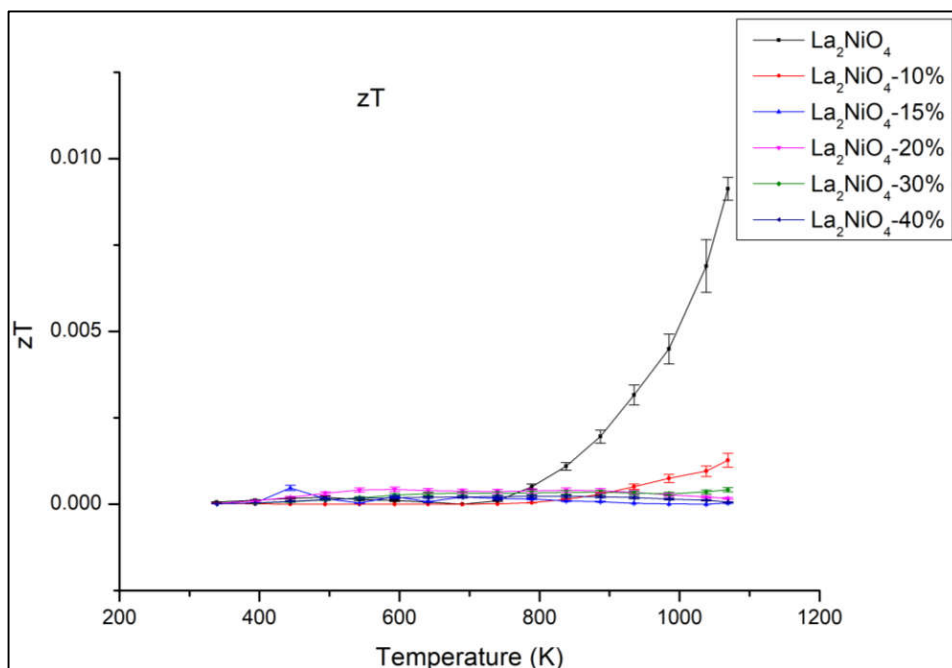

Fig. 21. Figure of merit ZT calculated at high temperatures for the La_2NiO_4 family of compounds.

The parent compound shows the largest value of ZT with a value of ~0.01 at 1073K. The ZT values of the doped compounds are much lower than that of the parent compound. This is mainly due to the low values of Seebeck coefficient shown by the doped compounds which could be due to the lack of charge carriers or low mobility or both as mentioned earlier.

3.2 $La_3Ni_2O_7$ Family

3.2.1 Structural Analysis

The structure of the parent compound $La_3Ni_2O_7$ was analysed using Rietveld refinement of the X-Ray Diffraction pattern of the sample. The pattern did not show any extra phases present and hence we can say that the synthesized compound is a phase pure compound. The $La_3Ni_2O_7$ phase exists in the orthorhombic Fmmm space group and this has been used to perform the Rietveld refinement for the room temperature as well as the high temperature X-Ray Diffraction patterns. Fig. 22 shows the Rietveld refinement fit of the powder X-Ray Diffraction pattern of $La_3Ni_2O_7$ taken at room temperature.
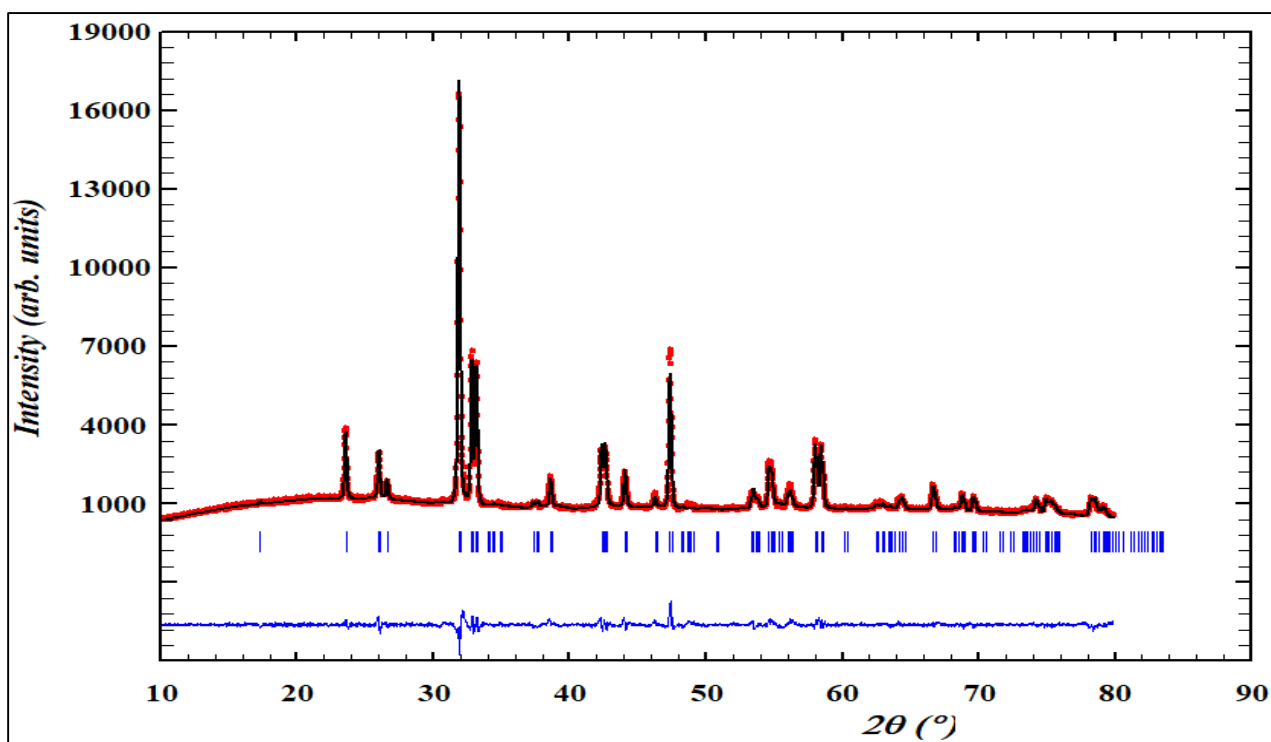
Fig. 22. Rietveld refinement fit (black line) of the powder X-Ray Diffraction pattern (red circles) of La$_3$Ni$_2$O$_7$ at room temperature. Blue stripes indicate the peak positions of La$_3$Ni$_2$O$_7$ and the blue line is the difference in the data and the fit.

Table V. X-Ray Diffraction data of La$_3$Ni$_2$O$_7$.

Chemical Formula Molecular Weight (in g/mol) Temperature (K)	La$_3$Ni$_2$O$_7$ 646.1 296
Crystal Structure	Orthorhombic
Space group symmetry	Fmmm
Unit Cell Parameters	
a (Å)	5.396(6)
b (Å)	5.451(1)
c (Å)	20.534(0)
α, β, γ (°)	90
V (Å^3)	604.053
Diffraction angle, 2θ (°)	10-79.9957
Step size, 2θ (°)	0.01038
R values	
R$_{wp}$	14.5
R$_e$	8.04
χ^2	3.23
Goodness of fit	1.80

Table V shows the calculated parameters from the Rietveld refinement of the diffraction data of $La_3Ni_2O_7$ at room temperature.

Table VI. Atomic positions and fractional occupancy in $La_3Ni_2O_7$ at room temperature.

Atom	a	b	c	Fractional Occupancy
La1	0	0	0.5	0.526(49)
La2	0	0	0.3197(2)	0.824(76)
Ni1	0	0	0.0791(9)	0.426(73)
O1	0	0	0	0.665(61)
O2	0	0	0.1072(1)	2.061(48)
O3	-0.25	0.25	0.0965(8)	2.017(24)

The atomic positions and fractional occupancy of $La_3Ni_2O_7$ are given in Table VI. The last digit in atomic positions and the last two digits in the fractional occupancy are uncertain. From the values of fractional occupancy calculated we can say that the compound might have a deficiency of oxygen present in its stoichiometry.

High temperature X-Ray diffraction patterns of the parent $La_3Ni_2O_7$ seems to show a change in phase at higher temperatures as seen in Fig. 23 but upon initial Rietveld refinement of the scans it was clear that there is no such phase transition. The compounds still exists in the same *Fmmm* space group across all the temperatures. Further refinement needs to be done to extract the lattice parameters of the compound.
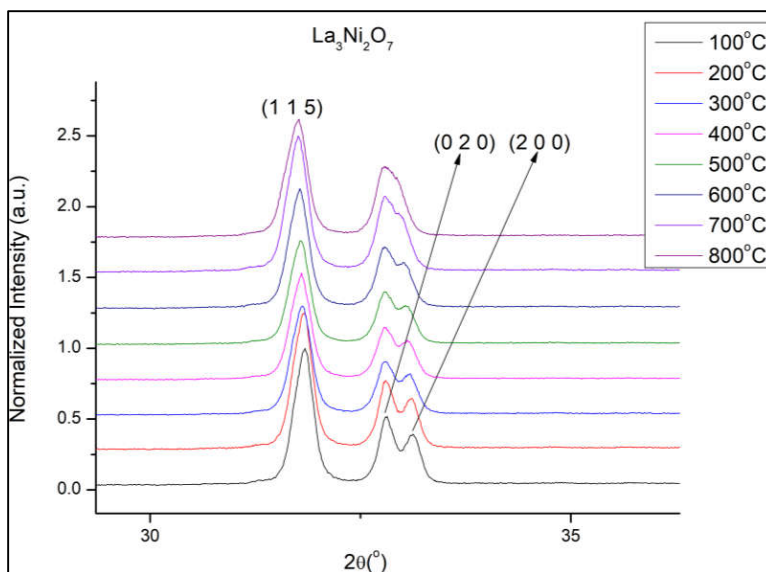

Fig. 23. High temperature X-Ray diffraction pattern of $La_3Ni_2O_7$ with their corresponding (hkl) values

A preliminary analysis of the X-Ray Diffraction patterns of the doped compounds showed the presence of La_2NiO_4 in the samples. Quantitative analysis of the secondary phase by Rietveld refinement has not been done yet.

3.2.2 Electrical properties

The average resistivity values are shown in Fig. 24 and the average Seebeck Coefficient values are shown in Fig. 25.

3.2.2.1 Electrical Resistivity
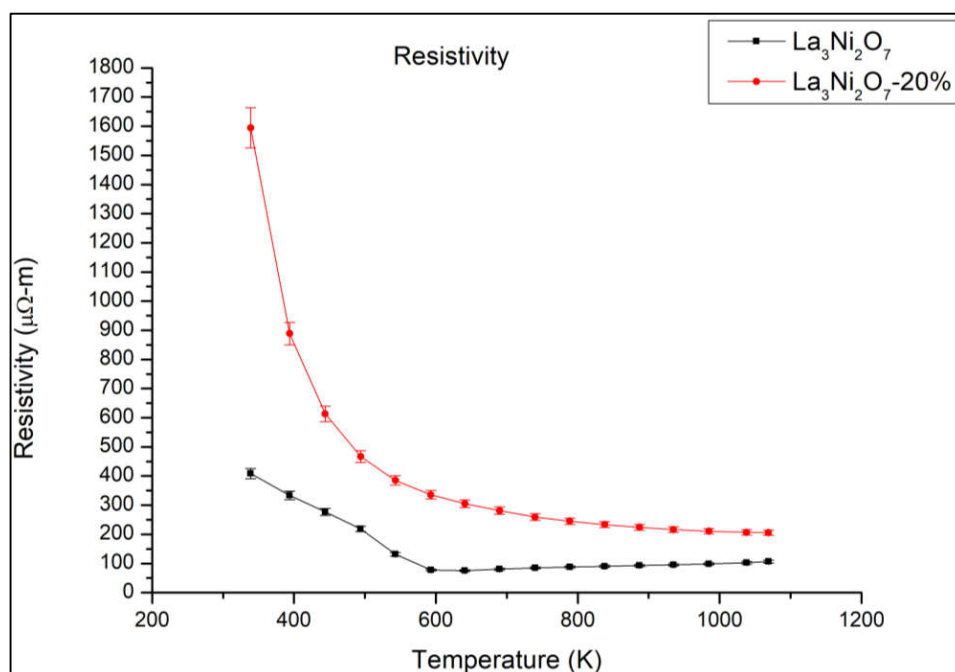
Fig. 24. Electrical resistivity at high temperatures for the $La_3Ni_2O_7$ parent and the 20 at.% doped compound.

The sudden dip in the resistivity of the parent at ~600K compound can suggest the presence of a phase transition that might have increased the mobility of the charge carriers. This is also seen in earlier reports of electrical conductivity[23] shown in Fig. 5. When compared with the values obtained for the La_2NiO_4 family, the resistivity values are lower. This is in agreement with the general trend of the Ruddlesden-Popper series mentioned earlier.[20] The increase in resistivity of the doped compound from the parent could also be the result of impurities present in the compound. Measurements for the remaining samples have to be done in order to look for a trend in the electrical behaviour of this family.

3.2.2.2 Seebeck Coefficient

The room temperature values of the parent compound are in agreement with previous reports.[20] The negative value of the Seebeck implies that electrons are the majority charge carriers in this system and the presence of a p-type Ca dopant has caused the Seebeck values to shift slightly to the positive side. The sudden increase in the Seebeck values for both compounds from ~600K could be an indication of a change in carrier concentration or mobility or both. High temperature Hall measurement is required to fully understand this behaviour.
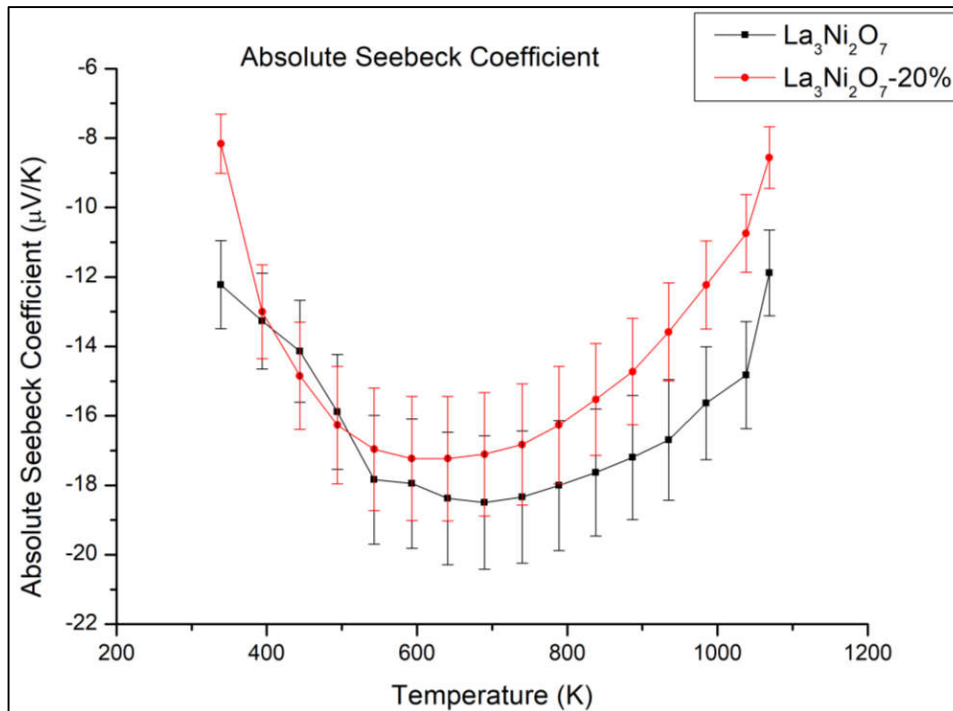
Fig. 25. Absolute Seebeck Coefficient at high temperatures for the $La_3Ni_2O_7$ parent and the 20 at.% doped compound.

3.2.2.3 Power Factor

The Power factor is calculated using the formula mentioned in equation 3.1. Fig. 26 shows the value of the Power Factor calculated from the Resistivity and Seebeck measurement done earlier.

The increase in resistivity as well as the decrease in magnitude of the Seebeck coefficient of the doped compound seen earlier has resulted in the reduction of its Power Factor. The sudden increase in the value of the Power Factor for the parent compound can be traced back to the abnormalities seen in the resistivity and Seebeck values of the parent compound at the same temperature. The structure of the both compounds at high temperatures needs to be studied

further to check for any structural change that might result in the abnormal behaviour seen in the data.

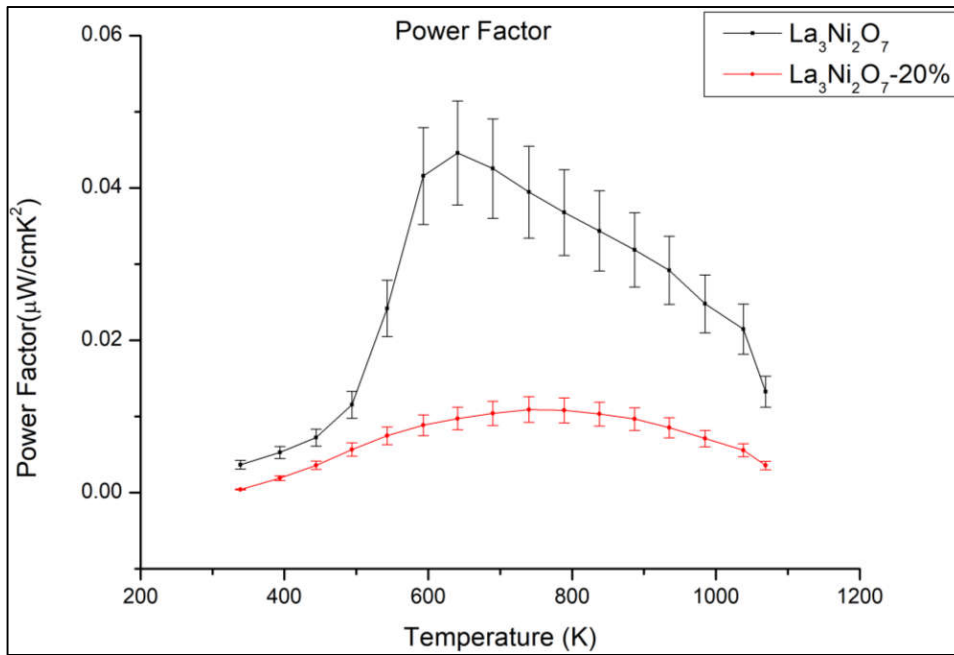**Fig. 26.** Power Factor calculated at high temperatures for the $La_3Ni_2O_7$ parent and the 20 at.% doped compound.

3.2.3 Thermal Properties

The average values of thermal conductivity values are shown in Fig. 27. The heat capacity value used in this calculation was 427.92 $JK^{-1}mol^{-1}$ taken from the study done by Nuri Solak. [35]

3.2.3.1 Total Thermal Conductivity

The total thermal conductivity (K_{total}) is the sum of the electronic thermal conductivity (K_e) and the lattice thermal conductivity (K_l). The values were calculated using equation 2.8 from the measured thermal diffusivity values and density of the sample.

K_{total} is seen to be decreasing with increasing temperature. Doping concentrations up to 30 at.% reduces the thermal conductivity values when compared with the corresponding values of the parent compound but 40 at.% Ca doped compound shows a drastic increase in the thermal conductivity. This could be due to the presence of impurities in the compound. Quantitative analysis of the impurities present in each compound has to be done before any generalization can be made. These values are larger than that of the La_2NiO_4 family which could be the result

of the change in lattice boundaries between the two systems that could have provided free movement for the phonons in the $La_3Ni_2O_7$ compound.

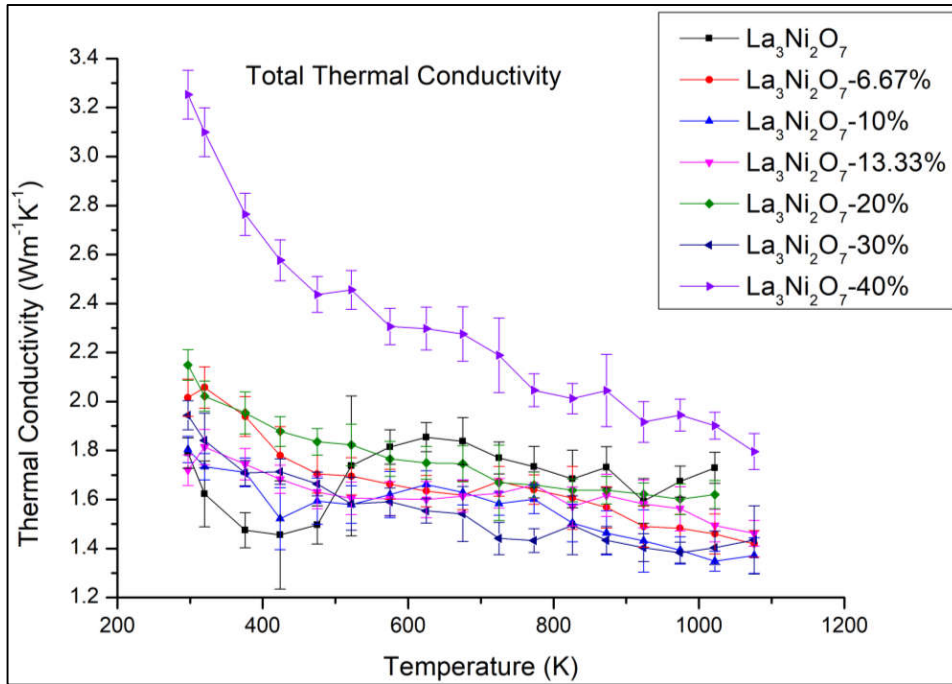**Fig. 27.** Total thermal conductivity measured and calculated at high temperatures for the $La_3Ni_2O_7$ family of compounds.

3.2.3.2 Electronic Thermal Conductivity

K_e was calculated using the formula mentioned in equation 3.2 derived from equation 1.3 where T is the temperature, ρ is the electrical resistivity and L is the Lorentz number which has a value of 2.44×10^{-8} $J^2K^{-2}C^{-2}$. Fig. 26 shows the plot of K_e against temperature calculated for the $La_3Ni_2O_7$ family.

The presence of the Ca dopant has reduced the electronic thermal conductivity as Ca was added as a p-type dopant with holes as the majority charge carriers which reduced the concentration of electrons similar to the La_2NiO_4 family. The sudden increase in K_e for the parent compound at ~600K might be due to phase transition suggested by the resistivity and Seebeck measurements. The values seen here are higher than that of the La_2NiO_4 family due to the increase in electron concentration in the system.

Fig. 28. Electronic thermal conductivity (K_e) calculated at high temperatures for the $La_3Ni_2O_7$ parent and the 20 at.% doped compound.

3.2.3.3 Lattice Thermal Conductivity

Lattice thermal conductivity (K_l) is the difference between K_{total} and K_e. Fig. 29 shows the calculated values of K_l.

K_l decreases steadily with increasing temperature for the doped compound. The sudden increase in K_l observed in the parent at ~600K suggests the presence of a structural phase transition around this temperature. This possibility is backed up heavily by the Seebeck and resistivity measurements as well. From this it is clear that the lattice thermal conductivity is more prominent than the electronic thermal conductivity. The larger value of the doped compound could be due to the presence of La_2NiO_4 or both.
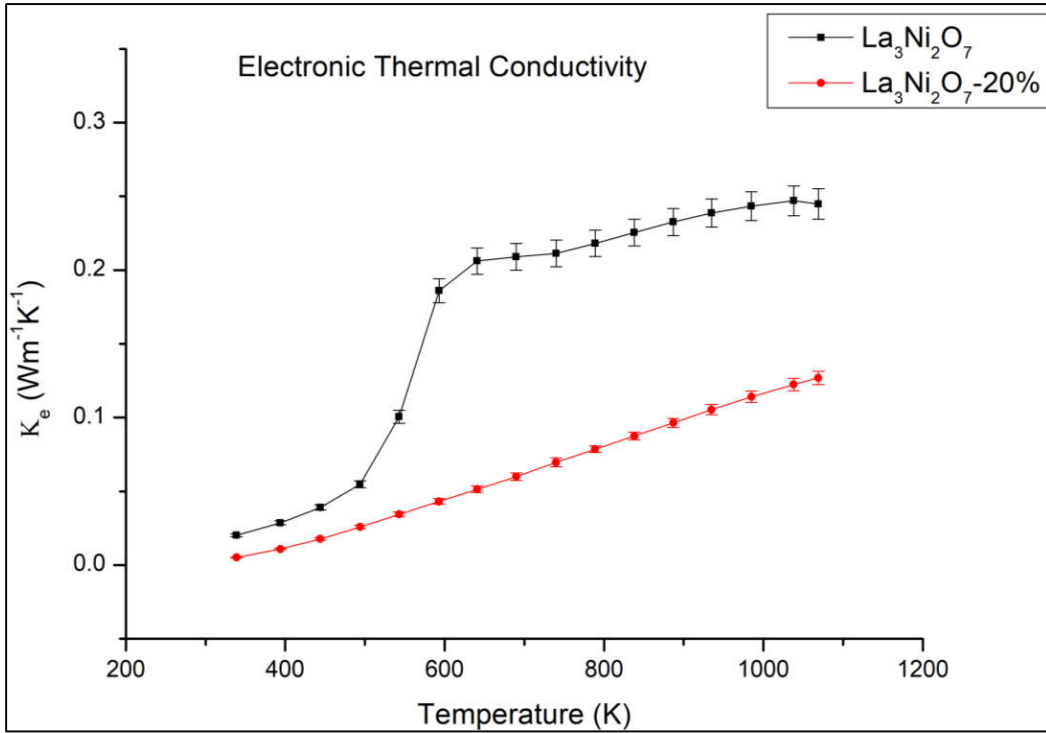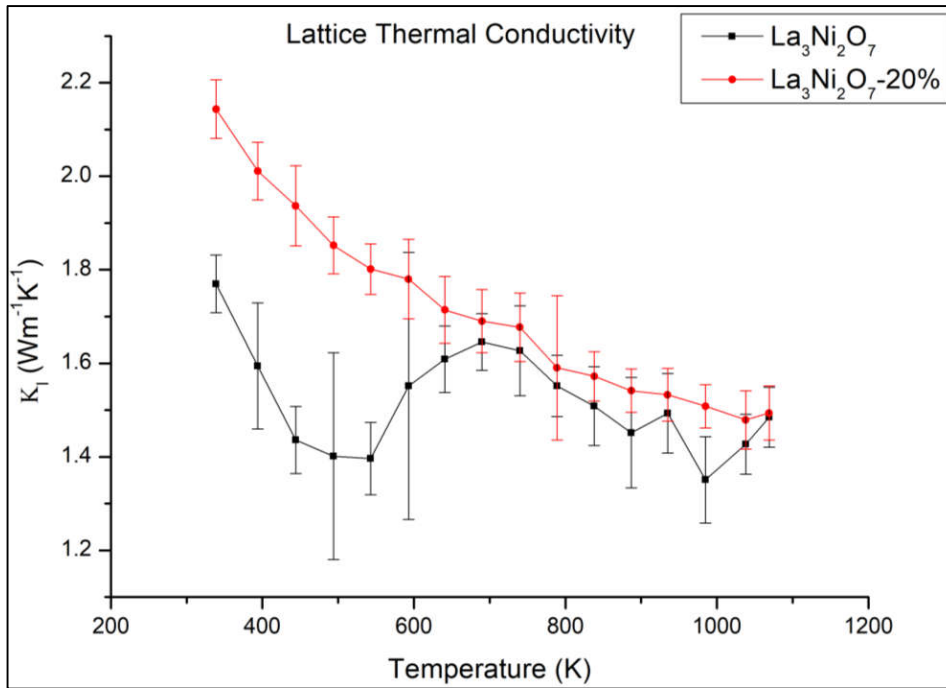
Fig. 29. Lattice thermal conductivity (K_l) calculated at high temperatures for the $La_3Ni_2O_7$ parent and the 20 at.% doped compound.

3.2.4 Figure of Merit zT

The overall figure of merit *zT* of the compounds is calculated using the formula given in equation 1.1. The calculated values of *zT* for this family are shown in Fig. 30.

The parent compound shows the largest value of *zT* with a value of ~0.00167 at 890K. The *zT* values of the doped compound is much lower than that of the parent compound. This is mainly due to the low magnitude of Seebeck coefficient shown by the doped compounds the possible reasons of which have been mentioned earlier. This low Seebeck value resulted coupled with the slight increase in thermal conductivity with respect to the La_2NiO_4 family has caused the value of zT to be significantly lower than that of the La_2NiO_4 family.

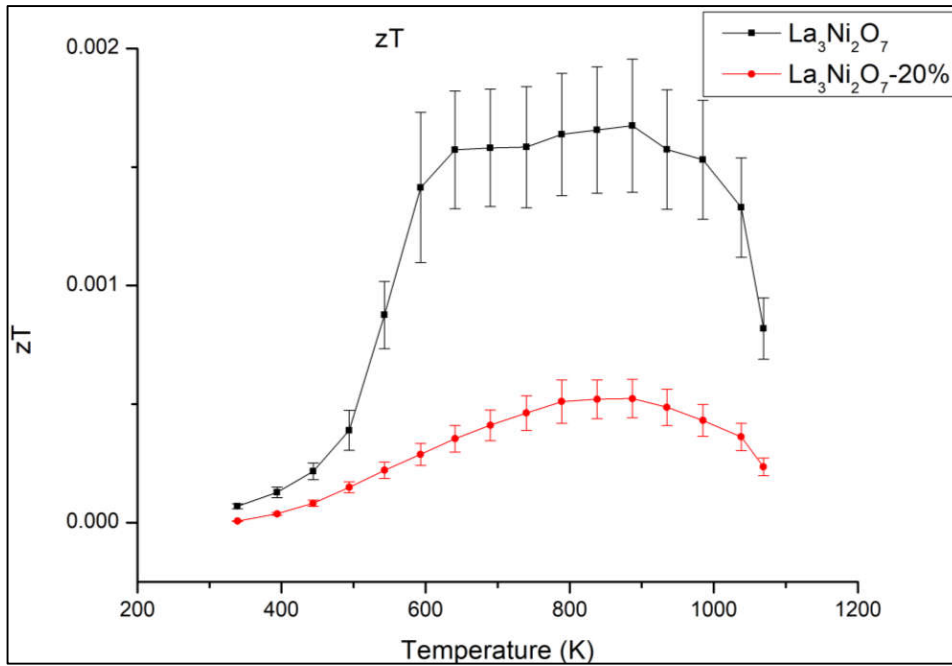**Fig. 30.** Figure of merit zT calculated at high temperatures for the $La_3Ni_2O_7$ parent and the 20 at.% doped compound.

3.3 Conclusion

La_2NiO_4 has a tetragonal crystal structure with *I4/mmm* space group. The high occupancy of oxygen suggests that there is an excess of oxygen present in this compound. Electrical resistivity values show a systematic decrease and Seebeck coefficient increases with increasing temperature. The presence of the dopant has increased the resistivity values and reduced the Seebeck coefficient. The resistivity values of the parent compound also match with the previously reported data. [16] The thermal conductivity measurements show a linear decrease in conductivity values at higher temperatures and a systematic increase with increasing dopant concentration up to 30 at% dopant. The maximum *zT* observed in this family is ~0.01 at 1069K shown by the parent compound.

$La_3Ni_2O_7$ has an orthorhombic crystal structure with *Fmmm* space group. The low occupancy of oxygen suggests that there is a deficit of oxygen in this compound. The presence of Ca dopant has increased the resistivity and decreased the magnitude of the Seebeck coefficient which is probably due to the presence of impurities in the doped compounds. It has also decreased the thermal conductivity except for the 40 at.% compound which has considerably increased the values of thermal conductivity at all temperatures when compared with the parent compound. A general trend of thermal conductivity against dopant concentration cannot be

studied without quantitatively estimating the amount of impurities present in the compound. The thermal conductivity decreases with increasing temperature except for the anomaly seen in the parent compound at ~600K. The parent compound shows the largest value of zT with a value of ~0.00167 at 890K.

3.4 Future Plans

- Complete the electrical transport measurements for the $La_3Ni_2O_7$ family and compute their overall figure of merit ZT.
- Perform Iodometric titration on the parent compound to estimate its oxygen content.
- High temperature Hall measurements have to be done to check the carrier concentration at high temperatures for all the compounds
- Synthesis and investigation of $(Fe_3O_4)_x(MgFe_2O_4)_{1-x}$ for potential thermoelectric properties.

References

[1] – G. Jeffrey Snyder and Eric S. Toberer, "Complex thermoelectric materials ", Nature Materials, **7**, 105 (2008.)

[2] – Slack, G. A. in CRC Handbook of Thermoelectrics (ed. Rowe, M.) 407–440 (CRC, Boca Raton, 1995).

[3] – Koumoto, K., Terasaki, I. & Funahashi, R., Complex oxide materials for potential thermoelectric applications, Material Research Society Bulletin **31**, 206–210 (2006).

[4] – Terasaki, I., Sasago, Y. & Uchinokura, K., Large thermoelectric power in $NaCo_2O_4$ single crystals, Physical Review Letters B **56**, 12685–12687 (1997).

[5] – Fitriani, R. Ovik, B.D. Long, M.C. Barma, M. Riaz, M.F.M. Sabri, S.M. Said and R. Saidur, A review on nanostructures of high-temperature thermoelectric materials for waste heat recovery, Renewable and Sustainable Energy Reviews **64**, 635–659 (2016).

[6] – Jeannine R. Szczech, Jeremy M. Higgins and Song Jin, Enhancement of the thermoelectric properties in nanoscale and nanostructured materials, Journal of Materials Chemistry **21**, 4037-4055 (2011).

[7] – Yifeng Wang, Kyu Hyoung Lee, Hiromichi Ohta, and Kunihito Koumoto, Thermoelectric properties of electron doped $SrO(SrTiO3)_n$ (n=1,2) ceramics, Journal of Applied Physics **105**, 103701 (2009).

[8] – Kunihito Koumoto, Yifeng Wang, Ruizhi Zhang,Atsuko Kosuga and Ryoji Funahashi, Oxide Thermoelectric Materials: A Nanostructuring Approach, Annual Review of Materials Research **40**, 363-394 (2010).

[9] – M. Ohtaki, T. Tsubota, K. Eguchi, and H. Arai, High-temperature thermoelectric properties of $(Zn_{1-x}Al_x)O$, Journal of Applied Physics **79**, 1816 (1996).

[10] – T. Tsubota, M. Ohtaki, K. Eguchi, and H. Arai, Thermoelectric properties of Al-doped ZnO as a promising oxide material for high-temperature thermoelectric conversion, Journal Materials Chemistry **7**, 85 (1997).

[11] – S. Katsuyama, Y. Takagi, M. Ito, K. Majima, H. Nagai, H. Sakai, K. Yoshimura, and K. Kosuge, Thermoelectric properties of $(Zn_{1-y}Mg_y)_{1-x}Al_xO$ ceramics prepared by the polymerized complex method, Journal of Applied Physics **92**, 1391 (2002).

[12] – M. Ohtaki, K. Araki, and K. Yamamoto, High thermoelectric performance of dually doped ZnO ceramics, Journal of Electronic Materials **38**, 1234 (2009).

[13] – H. Ohta, W.S. Seo, and K. Koumoto, Thermoelectric properties of homologous compounds in the $ZnO-In_2O_3$ system, Journal of American Ceramic Society **79**, 2193 (1996)

[14] – J. He, Y. Liu, R. Funahashi, Oxide thermoelectrics: The challenges, progress and outlook, Journal of Materials Research **26**, 1762–1772 (2011).

[15] – S Hébert, D Berthebaud, R Daou, Y Bréard, D Pelloquin, E Guilmeau, F Gascoin, O Lebedev and A Maignan, Searching for new thermoelectric materials: some examples among oxides, sulfides and selenides, Journal of Physics: Condensed Matter **28**, 013001 (2016)

[16] – lndu Bhushan Sharma and Devinder Singh, Solid State Chemistry of Ruddlesden-Popper type complex oxides, Bulletin of Materials Science **21**, 363-374 (1998)

[17] – S. N. Ruddlesden and P. Popper, New compounds of the K_2NiF_4 type, Acta Crystallographica **10**, 538-539 (1957)

[18] – S. N. Ruddlesden and P. Popper, The compound $Sr_3Ti_2O_7$ and its structure, Acta Crystallographica **11**, 54-55 (1958)

[19] – Rao C N R, Ganguly P, Singh K K and Mohan Ram R A, A comparative study of the magnetic and electrical properties of perovskite oxides and the corresponding two-dimensional oxides of K_2NiF_4 structure, Journal of Solid State Chemistry **72**, 14 (1988).

[20] – Sreedhar K, McElfresh M, Perry D, Kim D, Metcalf P and Honig, Low Temperature Electronic Properties of $La_{n+1}Ni_nO_{3n+1}$ (n=2,3 and ∞) system: Evidence for a crossover from Fluctuating-Valence to Fermi-Liquid-like behaviour, Journal of Solid State Chemistry **110**, 208 (1994)

[21] – Shingo Ohta, Takashi Nomura, Hiromichi Ohta, Masahiro Hirano, Hideo Hosono, and Kunihito Koumoto, Large thermoelectric performance of heavily Nb-doped $SrTiO_3$ epitaxial film at high temperature, Applied Physics Letters **87**, 092108 (2005)

[22] – Masahiro Yamamoto, Hiromichi Ohta and Kunihito Koumoto, Thermoelectric phase diagram in a $CaTiO_3$–$SrTiO_3$–$BaTiO_3$ system, Applied Physics Letters **90**, 072101(2007)

[23] – G. Amow, I.J. Davidson, S.J. Skinner, A comparative study of the Ruddlesden-Popper series, $La_{n+1}Ni_nO_{3n+1}$ (n=1, 2 and 3), for solid-oxide fuel-cell cathode applications, Solid State Ionics **177**, 1205–1210 (2006).

[24] – A. Demourgues, P. Dordor, J.-P. Doumerc, J.-C. Grenier,1 E. Marquestaut, M. Pouchard, Transport and Magnetic Properties of $La_2NiO_{4+\delta}$ (0≤δ≤0.25), Journal of Solid State Chemistry **124**, 199–204 (1996).

[25] – Yongna Shen, Hailei Zhao, Xiaotong Liu and Nansheng Xu, Preparation and electrical properties of Ca-doped $La_2NiO_{4+\delta}$ cathode materials for IT-SOFC, Physical Chemistry Chemical Physics **12**,15124–15131(2010).

[26] – Pikalova Elena Yurievna, Kolchugin Alexander Anatolievich, Bogdanovich Nina Mihailovna and Bronin Dimitry Igorevich, Electrical and Electrochemical Properties of La_2

$_x$Ca$_x$NiO$_{4+\delta}$ and La$_{2-x}$Ca$_x$NiO$_{4+\delta}$–Ce$_{0.8}$Sm$_{0.2}$O$_{1.9}$ Cathode Materials for Intermediate Temperature SOFCs, Advances in Science and Technology **93**, 25-30 (2014) .

[27] – Zhang Z and Greenblatt M, Synthesis, Structure and Physical properties of La$_{3-x}$M$_x$Ni$_2$O$_{7-\delta}$ (M = Ca^{2+}, Sr^{2+}, Ba^{2+}; 0<x≤0.075), Journal of Solid State Chemistry **111**, 141 (1994).

[28] – Singhka, W. and Kuharuangrong S, Synthesis and Physical Properties of La$_{3-x}$Sr$_x$Ni$_2$O$_{7\pm\delta}$ Ruddlesden-Popper Phase Journal of Metals, Materials and Minerals **18**, 77-82 (2008).

[29] – Sreedhar and Honig, Low Temperature Electron Transport Properties of La$_{2-x}$Sr$_x$NiO$_4$ with 0.5≤x≤1.3, Journal of Solid State Chemistry **111**, 147-150 (1994)

[30] – M. Zinkevich, F. Aldinger, Thermodynamic analysis of the ternary La–Ni–O system, Journal of Alloys and Compounds **375,** 147–161 (2004).

[31] – R. A. Young, The Rietveld Method, Oxford University Press, 1995

[32] – LINSEIS LFA-1000 Instruction Manual

[33] – Anna Judith Ellett, Oxygen Permeation and Thermo-Chemical Stability of Oxygen Separation Membrane Materials for the Oxyfuel Process, Section 8.4 (2010)

[34] – M. Castro, R. Burriel, Heat capacity study of La$_2$NiO$_4$ and Pr$_2$NiO$_4$, Thermochimica Acta **269/270,** 537-552 (1995).

[35] – Nuri Solak ,"Interface Stability in Solid Oxide Fuel Cells for Intermediate Temperature Applications", Doctoral Dissertation at University of Stuttgart (2007).

[36] – LINSEIS LSR-3 Instruction Manual

[37] – Iwanaga S., Toberer, E. S., LaLonde A. and Snyder G. J., A High Temperature Apparatus for Measurement of the Seebeck Coefficient, Review of Scientific Instruments **82**, 063905 (2011).

[38] – Wang H., Porter W. D., Bottner H., Konig J., Chen L., Bai S., Tritt T. M., Mayolet A., Senawiratne J., Smith C., Harris F., Gilbert P., Sharp J. W., Lo J., Kleinke H. and Kiss, L, Transport Properties of Bulk Thermoelectrics-An International Round-Robin Study, Part I: Seebeck Coefficient and Electrical Resistivity, Journal of Electronic Materials **42**, 654-664 (2013).

[39] – Mackey J., Dynys F. and Sehirlioglu A, Uncertainty Analysis for Common Seebeck and Electrical Resistivity Measurement, Systems. Review of Scientific Instruments **85**, 085119 (2014).